This article has been accepted for publication in a future issue of this journal, but has not been fully edited. Content may change prior to final publication. Citation information: DOI 10.1109/ACCESS.2017.2727819, IEEE Access



# Applications of Conformal Geometric Algebra to Transmission Line Theory

Alex Arsenovic[1]

[1]Eight Ten Labs LLC, Stanardsville Va, 22973

Corresponding Author: Alex Arsenovic (alex@810lab.com)

***Abstract*—In this paper we present the application of a projective geometry tool known as Conformal Geometric Algebra (CGA) to transmission line theory. Explicit relationships between the Smith Chart, Riemann Sphere, and CGA are developed to illustrate the evolution of projective geometry in transmission line theory. By using CGA, fundamental network operations such as adding impedance, admittance, and changing lines impedance can be implemented with rotations, and are shown to form a group. Additionally, the transformations relating different circuit representations such as impedance, admittance, and reflection coefficient are also related by rotations. Thus, the majority of relationships in transmission line theory are linearized. Conventional transmission line formulas are replaced with an operator-based framework. Use of the framework is demonstrated by analyzing the distributed element model and solving some impedance matching problems.**

## I. Introduction

### A. Context and Motivation

Complex numbers are ubiquitous in science and engineering mainly because they provide a powerful way to represent and manipulate rotations. Despite their usefulness, complex numbers are limited to rotations in two-dimensions. This is a serious drawback given that many problems in physics and engineering are inherently multi-dimensional. As a work-around, most high-dimensional problems are solved using matrices of complex numbers, effectively modeling a high-dimensional space using sets of 2D sub-spaces. While an amazing set of problems have been tackled using this technique, the solutions can be overly complicated and often miraculous. Furthermore, it produces theories and models that are difficult to understand and extend.

A better approach might be to use a high dimensional algebra for high dimensional problems. For it stands to reason that if the ability to efficiently handle rotations in two dimensions has been so successful in science and engineering, then a similar ability in higher dimensions should be even more so.

### B. Previous Work

Projective geometry has been used as a conceptual tool to generate various impedance charts since the 1930's [1]. Several such charts, including the Smith Chart, can be constructed using stereographic projection onto the Riemann Sphere. Although it has been known to microwave engineers for over 50 years, the Riemann sphere continues to spark interest [2]. Unfortunately, the inability of complex algebra to handle rotations in three-dimensional space makes the Riemann Sphere an impractical tool. In order to make use of projective geometry, a *higher* algebra is required. Quaternions can be used for three-dimensional applications such as the Riemann sphere, but they do not scale to four or higher dimensions. In addition, neither quaternions nor complex numbers are adequate tools for non-euclidean geometry, which is the natural geometry for several parts of transmission line theory [3].

Geometric Algebra (GA) subsumes complex algebra, quaternions, linear algebra and several other independent mathematical systems. Additionally, GA supports both arbitrary dimensions and non-euclidean geometries, making it an attractive tool for applications in transmission line theory. The usage of geometric algebra in electrical engineering was pioneered by E. F. Bolinder in the 1950s, and continued throughout his career [4]–[6]. Unfortunately, it does not appear that anyone directly extended his work. We attribute this to the complexity and specialization of his applications combined with the rapid development of the geometric algebra during his time. However, recently there has been a resurgence of interest in using GA in electrical engineering problems, as demonstrated by the invited cover article of the 2014 "Proceedings of the IEEE" entitled "Geometric Algebra for Electrical and Electronic Engineers" [7]. In part, this interest is due to the publication of application-oriented, comprehensive texts on the subject [8], [9], making geometric algebra more accessible to scientists and engineers than ever before.

### C. Outline

In this paper we present the application of the projective geometry tool known as Conformal Geometric Algebra (CGA) to transmission line theory. CGA is a specific construction in GA which is used to linearize conformal transformations. Although somewhat foreign to RF and Microwave engineers at this time, CGA has been successfully applied in the fields of computer graphics [10]–[12] and robotics [13].

Section II begins with a geometric interpretation of complex numbers, as used in linear system theory. This example is given to provide context and demonstrate that projective geometry is implicit in the conventional theory currently used by engineers. Once these observations are put forth, translation from complex algebra into geometric algebra begins. First, complex numbers representing values of reflection coefficient are translated into vectors of a two-dimensional geometric algebra. Next, the Smith Chart is mapped onto the Riemann Sphere using stereographic projection in Section III. The

This article has been accepted for publication in a future issue of this journal, but has not been fully edited. Content may change prior to final publication. Citation information: DOI 10.1109/ACCESS.2017.2727819, IEEE Access



sphere is used in Section IV to demonstrate that the different circuit representations are related by rotations of the sphere. Section V provides some example applications of the sphere. Various shortcomings associated with the Riemann Sphere are identified and this motivates the use conformal geometric algebra (CGA). The basics of CGA are briefly described and then its application to transmission line theory is presented in Section VI. This approach leads to the identification of a group structure present in the discrete circuit elements, and depicts their actions on the Smith Chart. The discrete element operators are used in Section VII to explore the distributed element model of a transmission line. It is shown that mismatched transmission lines produce non-euclidean rotations which encircle their characteristic impedance, and these are uniquely represented with CGA. Next, some simple impedance matching circuits are analyzed in Section VIII for demonstration. Section IX presents an argument for the adoption of CGA transmission line theory. This section can be read out of order, but is presented last so that some of the claims may be appreciated. Finally, the results are compiled in Section X and discussed.

Although a brief introduction to GA is given, fluency in geometric and conformal geometric algebra requires additional study. Comprehensive introductions to these subjects is beyond the scope of this article, and have been adequately presented elsewhere [8], [9], [14]. We hope that the results and arguments put forth incite a curiosity and desire in those unacquainted with the subject to learn more.

## II. Geometric Algebra and Projective Geometry

### A. Complex Numbers Linearize Phase Shifts

Engineers use complex numbers in a variety of creative ways. One of the most fruitful applications of complex numbers is to linearize the operation of phase shifting harmonic signals. This technique is used in linear system analysis, where arbitrary signals are represented by sums of harmonic signals. As is well known, given a harmonic excitation applied to a linear system, the response will be a harmonic signal of the same frequency but with a possible change in amplitude and phase shift. The effect of these transforms are represented graphically in Figure 1. From an operational perspective, linear time invariant (LTI) systems are operators limited to transforms of phase scaling and amplitude shifting, when acting upon harmonic signals.

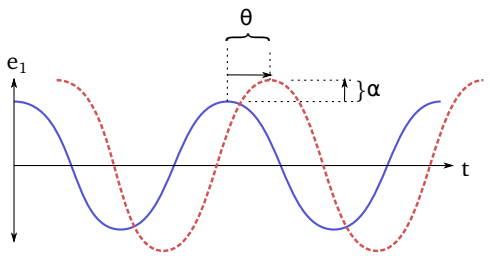


Figure 1: The effect of a linear system on a harmonic input signal.. The original solid sinusoid is phase shifted by $\theta$ and amplitude scaled by $\alpha$, producing the dashed sinusoid.

Since the effect of all linear systems is limited to these two transformations, it pays to represent them as concisely as possible in the algebra. The scaling operation is implemented by scalar multiplication, but the shift operation requires a trick. Referring to Figure 2; first, a new dimension ($e_2$) is added orthogonal to the existing two, producing 3-dimensional space. Next, the sinusoid is modeled as the perpendicular projection of a helix. Given this construction, it can be seen that rotating the helix about its longitudinal axis produces a phase shift in the projection of the sinusoid. Thus, we have replaced a shift operation with a rotation in a plane. Finally, by recognizing that a linear system may be represented by the transformation itself, the sinusoid may be forgotten, and the rotation and scaling information retained.

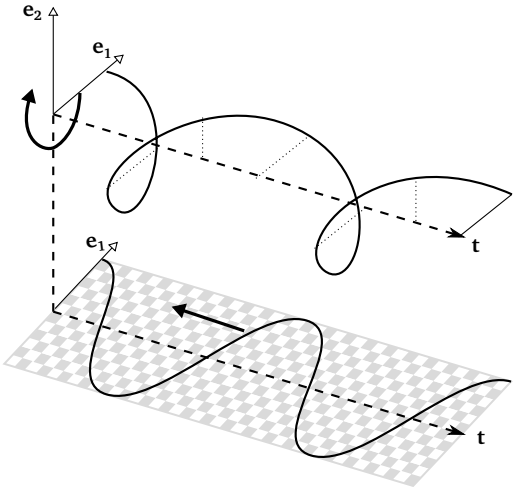


Figure 2: Rotating a helix about the longitudinal axis creates a phase shift in the projected sinusoid.

### B. The Need for Higher Dimensions

In microwave engineering, and other disciplines rooted in wave-mechanics, the mathematical operations required to describe a system extend beyond shift and scale. However, most of the required operations for transmission line analysis are Möbius transformations. Therefore, the ability to represent Möbius transformations with rotations should provide a great increase in algebraic efficiency. As has been well documented by David Hestenes and others [8], [9], [15], this can be done using Conformal Geometric Algebra (CGA). Frequently, CGA is introduced by way of stereographic projection [8]. This approach provides a transitional geometry between the original two-dimensional euclidean space and the four-dimensional Minkowski space of CGA. Additionally, it illustrates how the Riemann sphere naturally fits into the scheme. The relationship of the algebras from the complex plane to CGA may be expressed,

$$\underbrace{\mathbb{C} \Longrightarrow G_2}_{\text{Smith Chart}} \longrightarrow \underbrace{G_3}_{\text{Riemann Sphere}} \longrightarrow \underbrace{G_{3,1}}_{\text{CGA}}. \qquad (1)$$

Before stereographic projection into three-dimensional space can be done efficiently, Geometric Algebra has to be adopted. Therefore, we start by translating complex algebra

This article has been accepted for publication in a future issue of this journal, but has not been fully edited. Content may change prior to final publication. Citation information: DOI 10.1109/ACCESS.2017.2727819, IEEE Access



into geometric algebra, and then move onto the Riemann Sphere and its relationship to the Smith Chart.

### C. Introduction to Geometric Algebra

Geometric Algebra introduces new types of mathematical objects and operators beyond those defined by complex or vector algebra. In this section we introduce some basic concepts, but move on quickly to the application at hand. A good introduction to GA aimed at electrical engineers can be found in the article by Chappell et. al. [7], but those seeking a comprehensive introduction to GA can refer to the first two chapters of [8] or the first part of [9].

Given a set of vectors which span a space, the elements of the corresponding geometric algebra are generated by employing a product known as the *outer product*, denoted with a wedge: $\wedge$. The outer product between two non-parallel vectors produces a new kind of element called a *bivector*. Just as vectors represent directed length, bivectors represent directed areas. In a similar way, the outer product of three vectors creates a trivector, four vectors create a quadvector, and so on. An illustration of these elements and the vectors which generate them is shown in Figure 3. Various N-vectors can be combined to form a single multivector, analogous to the way complex numbers combine real and imaginary parts. Geometric concepts such as quantities, operators, and subspaces are represented by objects within the algebra and this produces clarity and concision.

Many results of Geometric Algebra follow intuitively once commutativity it abandoned. Start by assuming that the square of a vector is a scalar and that the addition of two vectors produces another vector. We can then write

$$(a+b)^2 = a^2 + b^2 + 2\,(ab + ba)\,. \tag{2}$$

So the quantity $(ab + ba)$ must be a scalar. Define this symmetric product as the *inner* product, which is a familiar concept.

$$a \cdot b \equiv \frac{1}{2}\,(ab + ba) \tag{3}$$

Next, separate the product of two vectors into symmetric and asymmetric parts

$$ab = \underbrace{\frac{1}{2}\,(ab + ba)}_{\text{symmetric}} + \underbrace{\frac{1}{2}\,(ab - ba)}_{\text{asymmetric}}\,. \tag{4}$$

Since commutativity is not assumed, we are forced to interpret the asymmetric part, so define the *outer* product to be

$$a \wedge b \equiv \frac{1}{2}\,(ab - ba)\,. \tag{5}$$

Given $a \wedge a = 0$, the outer product can be interpreted as the measure of collinearity, analogous to the inner product as a measure of perpendicularity. The outer product can be interpreted as the oriented area swept out by sliding one vector along the other, as shown in Figure 3. Combining both inner and outer product into a single balanced product known as the *geometric product* gives the algebra substantial power and allows for vector inersion. The three products are related by the fundamental equation,

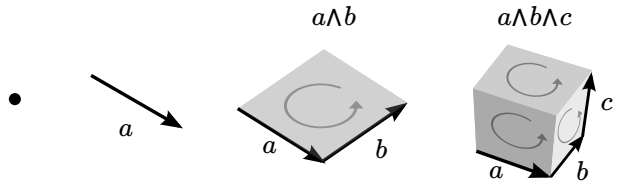


Figure 3: Interpretation of some elements within Geometric Algebra, highlighting their creation through the use of the outer product. From left to right there is; a scalar, vector, bivector and tri-vector.

$$ab = a \cdot b + a \wedge b. \tag{6}$$

The workings of GA are best understood with some examples, so the next section introduces the geometric algebra of a plane. This algebra will be used to translate complex numbers into our model.

### D. The Plane

Given a two-dimensional GA with the orthonormal basis,

$$e_i \cdot e_j = \delta_{ij}. \tag{7}$$

The geometric algebra consists of scalars, two vectors, and a bivector,

$$\{\underbrace{\alpha}_{\text{scalar}}, \quad \underbrace{e_1, e_2}_{\text{vectors}}, \quad \underbrace{e_1 \wedge e_2}_{\text{bivector}}\}. \tag{8}$$

An illustration of the algebra and it's basis is shown in Figure 4. The highest dimensional element in a geometric algebra is commonly referred to as the *pseudoscalar*, which in this case is a bivector. Note that due to the orthogonality, the geometric product between the two basis vectors is equivalent to the outer product,

$$e_1 e_2 = e_1 \cdot e_2 + e \wedge e_2 = e_1 \wedge e_2. \tag{9}$$

And since the outer product is asymmetric, interchanging the order of a series of vectors in a product changes it's sign.

$$e_1 e_2 = -e_2 e_1 \tag{10}$$

Using these properties it can be seen that left multiplying a vector by the bivector rotates it clockwise $90°$.

$$(e_1 \wedge e_2)\, e_1 = e_1 e_2 e_1 = -e_1^2 e_2 = -e_2 \tag{11}$$

Right multiplying a vector by the bivector rotates it counter-clockwise by $90°$.

$$e_1\,(e_1 \wedge e_2) = e_1 e_1 e_2 = e_1^2 e_2 = e_2 \tag{12}$$

And, the bivector squares to $-1$.

$$(e_1 \wedge e_2)^2 = e_1 e_2 e_1 e_2 = -1 \tag{13}$$

This article has been accepted for publication in a future issue of this journal, but has not been fully edited. Content may change prior to final publication. Citation information: DOI 10.1109/ACCESS.2017.2727819, IEEE Access



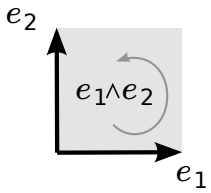


Figure 4: Geometric Algebra for a plane, illustrating the basis elements. $e_1$ and $e_2$ are vectors, and $e_1 \wedge e_2$ is a bivector.

Because of this property, the bivector can be used to replace the unit imaginary. For concision, bivector elements will be written with paired subscripts as such,

$$e_{12} \equiv e_1 e_2. \tag{14}$$

### E. Projections, Reflection, and Rotations

A major advantage of GA is that operators are represented as elements within the algebra. Since the geometric product between two vectors contains all the information regarding their relative directions, it can be used to define projections. By multiplying the vector $a$ with the square of a unit vector $n$, it can be decomposed into parts parallel and perpendicular to $n$.

$$a = an^2 = (an)\, n = \underbrace{(a \cdot n)\, n}_{a_\parallel} + \underbrace{(a \wedge n)\, n}_{a_\perp} \tag{15}$$

The parallel component is the *projection* of $a$ onto $n$, while the perpendicular component is the *rejection* of $a$ from $n$. This formula can be used in the computation of reflections. The reflection of a vector $a$ in the hyperplane perpendicular to the normalized vector $n$ is

$$a' = -nan. \tag{16}$$

To prove that this is a reflection, decompose $a$ into parts parallel and perpendicular to $n$, and note that the parallel component commutes with $n$ while the perpendicular component anti-commutes with $n$.

$$\begin{aligned} -nan &= -n\left(a_\perp + a_\parallel\right) n \\ &= -na_\perp n - na_\parallel n \\ &= n^2 a_\perp - n^2 a_\parallel \\ &= a_\perp - a_\parallel \end{aligned} \tag{17}$$

Which is a reflection in the hyperplane normal to $n$. Rotations can be constructed by cascading two reflections, but we just present the formulas directly since electrical engineers are familiar with complex numbers. Because $e_{12}$ squares to $-1$, we can use Euler's identity to write,

$$Z = e^{\theta e_{12}} = \cos\theta + \sin\theta e_{12}. \tag{18}$$

This is an example of a rotation operator known as a *rotor* in GA, and it *acts* through the geometric product. For example, to rotate the vector $e_1$ clockwise by angle $\theta$ we form

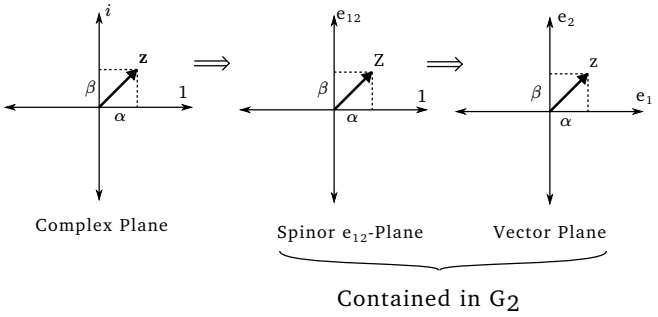


Figure 5: Map between the complex plane, spinor $e_{12}$-plane, and a vector plane.

$$Ze_1 = e^{\theta e_{12}} e_1 = \cos\theta e_1 - \sin\theta e_2. \tag{19}$$

While this formula works in two dimensions, rotations in three dimensions and above require a double-sided, half-angle formula so it is best to adopt it from the beginning. The same rotation expressed with the double-sided formula becomes,

$$e^{\frac{\theta}{2} e_{12}} e_1 e^{-\frac{\theta}{2} e_{12}} = \cos\theta e_1 - \sin\theta e_2. \tag{20}$$

A frequently used algebraic operation is to reverse the order of all vectors within a product, known as *reversion* and represented with a tilde (~). The reverse of a rotor is computed to be,

$$\tilde{Z} = \cos\theta + \sin\theta \tilde{e_{12}} = \cos\theta - \sin\theta e_{12}. \tag{21}$$

Using this notation, the rotation of a vector $a$ by a rotor $Z$ is written,

$$a' = Za\tilde{Z}. \tag{22}$$

If the rotor has a magnitude other than unity, it will affect a scaling operation as well as a rotation. In this case, the operator is called a *spinor*. The next section shows how complex numbers can be identified as spinors in a two-dimensional geometric algebra, and mapped into vectors.

### F. Translating Complex Numbers

To keep different objects in the various algebras distinct, we write complex numbers in bold face lower-case: $\mathbf{z}$, GA vectors in italic: $z$, and spinors/multivectors in uppercase italic: $Z$. Scalars in all algebras are equivalent, and are represented with greek italics, $\alpha, \beta$, unless agreement with existing theory demands otherwise. In complex algebra there is no distinction between rotation/dilation operators and vectors. However, in GA, vectors are vectors and rotation/dilation operators are spinors. Choosing which object to map a complex number onto is a design choice. We choose to model impedance, admittance, and reflection coefficient values as vectors, while the effects of changing domains or adding circuit elements are modeled as spinors.

The conversion from complex numbers to vectors is done in two steps. First, complex numbers are identified as the spinors

This article has been accepted for publication in a future issue of this journal, but has not been fully edited. Content may change prior to final publication. Citation information: DOI 10.1109/ACCESS.2017.2727819, IEEE Access



of a two-dimensional GA. These spinors can be transformed into vectors by choosing a reference direction. Graphically, this can be visualized as a map between the complex plane, the spinor plane, and the vector plane, as illustrated in Figure 5. Given the geometric algebra for a plane defined in the previous section, a complex number can be directly associated with a 2D spinor in the $e_{12}$-plane,

$$\underbrace{\mathbf{z} = \alpha + \beta i}_{\text{complex number}} \quad \Longrightarrow \quad \underbrace{Z = \alpha + \beta e_{12}}_{\text{2D spinor}}. \tag{23}$$

The spinor is then mapped to a vector by choosing a reference direction. This may be done by left multiplying with $e_1$.

$$Z \Longrightarrow e_1 Z = e_1\alpha + \beta e_1 e_{12} = \underbrace{\alpha e_1 + \beta e_2}_{\text{vector}}. \tag{24}$$

Although trivial, the need for this explicit map is useful when translating operations on the complex numbers to their vector equivalents. For example, complex conjugation translates to reversion of the spinor, which in turn translates into reflection of the vector in the hyperplane normal to $e_2$.

$$\mathbf{z}^\dagger = \alpha - \beta i \Longrightarrow \tilde{Z} = \alpha - \beta e_{12} \tag{25}$$

$$e_1 \tilde{Z} \Longrightarrow \alpha e_1 - \beta e_2 = -e_2 z e_2 \tag{26}$$

Additionally, complex inversion differs from vector inversion by a reflection in the hyperplane normal to $e_2$.

$$\mathbf{z^{-1}} = \frac{\mathbf{z}^\dagger}{\mathbf{z}^\dagger \mathbf{z}} = \frac{\mathbf{z}^\dagger}{|\mathbf{z}|^\mathbf{2}} \Longrightarrow \frac{\tilde{Z}}{|Z|^2} \tag{27}$$

$$e_1 \frac{\tilde{Z}}{|Z|^2} \Longrightarrow -e_2 z^{-1} e_2 \tag{28}$$

When a complex number is associated with a spinor, a rotation orientation ( clockwise vs counter clockwise) must be chosen. We choose to represent rotations by the conventions used in [8],

$$z' = R z \tilde{R}. \tag{29}$$

Given this choice, a counterclockwise rotation by $\theta$ in the $e_{12}$-plane is accomplished by the spinor,

$$R = e^{\frac{\theta}{2} e_{12}}. \tag{30}$$

Therefore the relation between a rotation in complex algebra and spinors is

$$\mathbf{z}' = e^{-\theta j}\mathbf{z} \quad \Rightarrow \quad z' = e^{\frac{\theta}{2} e_{12}} z e^{-\frac{\theta}{2} e_{12}}. \tag{31}$$

The rotation orientation of complex number aligns with the reversed rotor on the right-hand side of the formula.

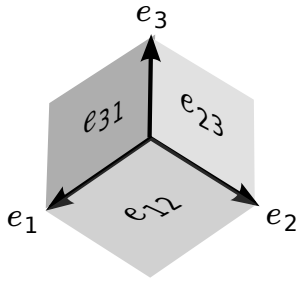


Figure 6: Geometric algebra for three dimensional space, illustrating the vector and bivector basis.

## III. The Riemann Sphere

### A. Introduction

Solving transmission line problems in terms of reflection coefficient is advantageous because passive devices are confined to a closed space, the unit circle. This removes the singularities produced by ideal shorts and open circuits in the impedance or admittance domain. By overlaying the contours of the Smith Chart onto the unit circle, the operations of adding impedance and admittance can be handled graphically. The result is a highly efficient nomogram which can be used to visualize and compute how various circuit elements alter the reflection coefficient.

Extending this approach, the Riemann Sphere constrains both passive and active devices to a closed space, the unit sphere. More importantly, it allows the transformation between impedance, admittance and reflection coefficient to be accomplished through rotations. The Riemann Sphere, as it relates to the Smith Chart, has been explored by a variety of researchers [1], [2], [16]. However, it does not share the widespread adoption similar to the Smith Chart. Perhaps this is due to the increase in geometric complexity without a sufficiently rich algebra, or perhaps because spheres are hard to draw!

### B. Geometric Algebra of Three Dimensional Space

This section introduces the geometric algebra of three dimensional space so that it can be used to work with the Riemann Sphere. Starting with an orthonormal vector basis defined by,

$$e_i \cdot e_j = \delta_{ij}. \tag{32}$$

The geometric algebra of space is generated and contains the following elements,

$$\underbrace{\alpha}_{1-\text{scalar}}, \underbrace{e_i}_{3\text{-vectors}}, \underbrace{e_{ij}}_{3-\text{bivectors}}, \underbrace{e_{123}}_{1\text{-trivector}}. \tag{33}$$

Again, the term *pseudoscalar* is used to describe the highest dimensional blade in any geometric algebra, which in this case is a tri-vector. An illustration of the vector and bivector basis is shown in Figure 6. The geometric algebra can be used to define projections, reflections, rotations, and all other vector algebra operations, but we limit our attention to rotations. First, note that each bivector squares to minus one,

This article has been accepted for publication in a future issue of this journal, but has not been fully edited. Content may change prior to final publication. Citation information: DOI 10.1109/ACCESS.2017.2727819, IEEE Access



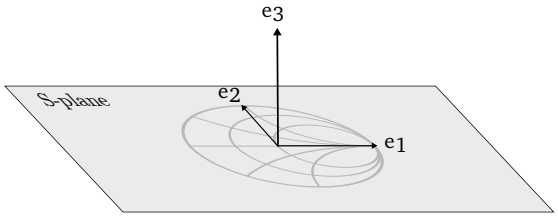


Figure 7: Vector Basis Set for the Smith Sphere

$$e_{12}^2 = e_{23}^2 = e_{31}^2 = -1. \tag{34}$$

When bivectors are multiplied together they return bivectors.

$$e_{12}e_{23} = -e_{31} \tag{35}$$
$$e_{12}e_{31} = -e_{21} \tag{36}$$
$$e_{31}e_{12} = -e_{23} \tag{37}$$

These multiplication rules may be recognized as those of the quaternion algebra, and indeed quaternions are nothing more than spinors of a three dimensional space. The beauty is that rotations can be implemented in an identical way as in two-dimensions. To demonstrate, take a vector $a = e_1 + e_2 + e_3$ and rotate it in the $e_{12}$-plane by an angle $\theta$.

$$a' = e^{\frac{\theta}{2}e_{12}} a e^{-\frac{\theta}{2}e_{12}} \tag{38}$$
$$= e^{\frac{\theta}{2}e_{12}} \left(e_1 + e_2 + e_3\right) e^{-\frac{\theta}{2}e_{12}} \tag{39}$$

To compute the result the rotor can be distributed to each component individually and then combined to form the total result. Doing this illustrates how vectors within the plane of rotation are affected, while vectors orthogonal to the plane of rotation are left invariant. Computing the rotation of each component,

$$e^{\frac{\theta}{2}e_{12}} e_1 e^{-\frac{\theta}{2}e_{12}} = \cos\theta e_1 - \sin\theta e_2 \tag{40}$$
$$e^{\frac{\theta}{2}e_{12}} e_2 e^{-\frac{\theta}{2}e_{12}} = \cos\theta e_2 + \sin\theta e_1 \tag{41}$$
$$e^{\frac{\theta}{2}e_{12}} e_3 e^{-\frac{\theta}{2}e_{12}} = e_3. \tag{42}$$

Finally, sum the components to form the final result.

$$a' = \left(\cos\theta + \sin\theta\right) e_1 + \left(\cos\theta - \sin\theta\right) e_2 + e_3 \tag{43}$$

Rotations of this sort will be used extensively in the applications to follow.

### C. Stereographic Projection

Stereographic projection onto the Riemann Sphere is a well known procedure but we will review it to make clear our notation and demonstrate the concision of geometric algebra. Beginning with a plane representing the reflection coefficient domain, the conventional contours familiar to Smith Chart users are drawn. This plane is spanned by the orthonormal vectors $e_1$ and $e_2$, as shown in Figure 7. These vectors correspond to the real and imaginary components of complex number as described in the previous section. Due to use of s-parameters in multi-port network analysis, we label the reflection coefficient plane the S-plane.

From the $e_{12}-$plane, an additional dimension is added perpendicular to the existing two labeled $e_3$ producing a three-dimensional geometric algebra, as defined in the previous section. To eliminate the added degree of freedom, the entire S-plane is mapped to the surface of a unit sphere through stereographic projection, defined as follows. Let $s$ be a point in the S-plane and $p$ be the corresponding point lying on the surface of the unit sphere. A ray connecting the projection point $e_3$ to the point in the S-plane '$s$' is drawn, as illustrated in Figure 8. The intersection of the ray with the surface of the sphere defines $p$. When $|s| < 1$, the ray is be projected through the S-plane, onto the interior of the sphere.

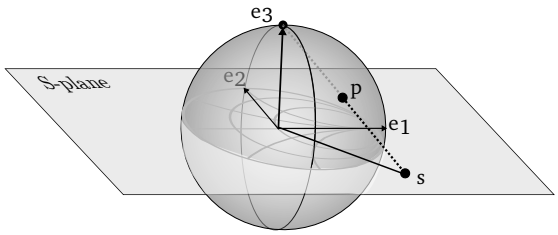


Figure 8: Stereographic projection of reflection coefficient plane (s-plane) onto Riemann Sphere. The point $s$ in the plane is mapped to the point $p$ on the sphere.

### D. Projection Up to Sphere

The first step is to determine $p$ given $s$. From Figure 8 it is geometrically obvious that

$$p = e_3 + \lambda\left(s - e_3\right), \tag{44}$$

where $\lambda$ is some scalar. The condition that $p$ lie on a unit sphere as well as orthonormal condition on $e_3$ provides the following constraints,

$$p^2 = 1 \qquad e_3^2 = 1 \qquad e_3 \cdot s = 0. \tag{45}$$

Enforcing these conditions allows $\lambda$ to be found,

$$\begin{aligned} p \cdot p &= \left(e_3 + \lambda\left(s - e_3\right)\right) \cdot \left(e_3 + \lambda\left(s - e_3\right)\right) \\ 1 &= 1 + \lambda^2\left(s^2 + 1\right) - 2\lambda \\ \lambda &= \frac{2}{s^2 + 1}. \end{aligned} \tag{46}$$

Putting this back into eq (44) provides the functional relationship for a point on the sphere in terms of a point on the S-plane.

$$p = \uparrow(s) \equiv e_3 + \frac{2}{s^2 + 1}\left(s - e_3\right) \tag{47}$$

Although the proof was based on geometry of mapping a plane to a sphere, the result holds true for any dimension [8]. Equation (47) may be re-arranged to separate components in the original plane and added dimension.

$$\uparrow(s) = \left(\frac{s^2 - 1}{s^2 + 1}\right) e_3 + \left(\frac{2}{s^2 + 1}\right) s \tag{48}$$

This article has been accepted for publication in a future issue of this journal, but has not been fully edited. Content may change prior to final publication. Citation information: DOI 10.1109/ACCESS.2017.2727819, IEEE Access



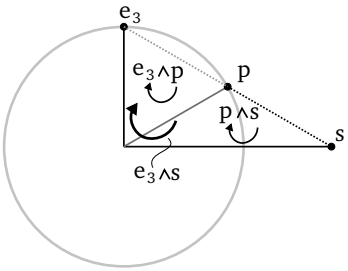


Figure 9: Relationship of bivectors involved in stereographic projection.

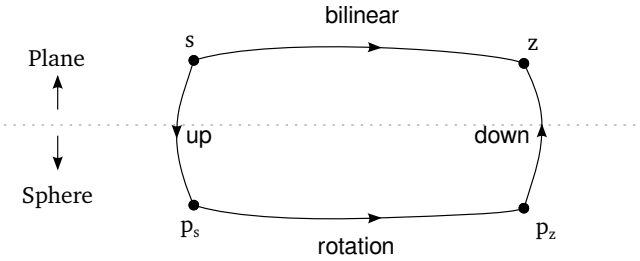


Figure 10: Commutative diagram illustrating the purpose of Stereographic projection.

### E. Projection Down to Plane

The second step in stereographic projection is to map a point on the sphere back to a point on the plane. Begin by observing that points $e_3, p$, and $s$ are collinear, as expressed by

$$e_3 \wedge p + p \wedge s = e_3 \wedge s. \tag{49}$$

This bivector equation may be illustrated by drawing a 2D slice of the sphere defined by $e_3$ and $s$, as shown in Figure 9. Next, decompose $p$ into components parallel and perpendicular to $e_3$.

$$p = \underbrace{e_3 \left(e_3 \cdot p\right)}_{p_\parallel} + \underbrace{e_3 \left(e_3 \wedge p\right)}_{p_\perp} \tag{50}$$

Using this in (49),

$$\begin{aligned} e_3 \wedge \left(p_\parallel + p_\perp\right) + \left(p_\parallel + p_\perp\right) \wedge s &= e_3 \wedge s \\ e_3 p_\perp + p_\parallel s &= e_3 s. \end{aligned} \tag{51}$$

Multiplying by $e_3$ and solving for $s$, we find

$$s = \downarrow (p) \equiv \frac{e_3 \left(e_3 \wedge p\right)}{1 - e_3 \cdot p}. \tag{52}$$

This formula can be interpreted as the rejection of $p$ from $e_3$, normalized by a factor of $(1 - e_3 \cdot p)$. It should be recognized that while we have used the variable $s$ to represent a point on the S-plane, these formulae hold true regardless of the interpretation of the plane.

## IV. Circuit Transformations

Once the functional relationship between the plane and sphere are known, operations within the plane can be translated into operations on the sphere. In this section the transformations between reflection coefficient, impedance, and admittance are shown to be implemented by rotations of the sphere. The commutative diagram shown in Figure 10 illustrates the scheme.

### A. S-to-Z

Instead of immediately resorting to mathematical proof, the relationship between reflection coefficient and impedance can be deduced geometrically by inspecting some values in both domains. Up-projecting the points $\pm 1, 0$, and $\infty$ to the sphere gives the north/south and east/west poles meaningful values. By labeling each pole with the corresponding normalized impedance value, as shown Figure 11, a pattern arises. The observed relationship between the $s$ and $z$ at the poles suggest that these two representations are related by a $90^\circ$ rotation in the $e_{13}$-plane.

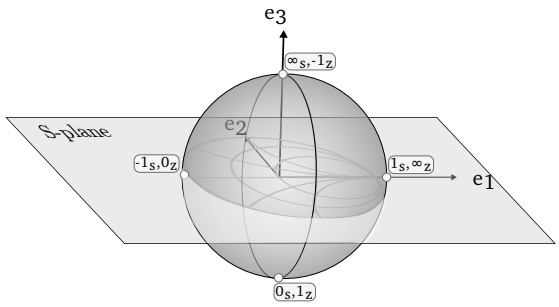


Figure 11: The Smith Chart mapped to the Riemann sphere. The poles in the $e_{13}$-plane labeled with values in both reflection coefficient $s$, and impedance $z$-domains.

To test this hypothesis, start with the point $p_s$ in terms of $s$,

$$p_s = e_3 + \frac{2}{s^2 + 1}\left(s - e_3\right). \tag{53}$$

Rotate the point by $90^\circ$ in the $e_{13}$ plane, producing $p_z$.

$$\begin{aligned} p_z &= e^{-\frac{\pi}{4} e_{13}} p_s e^{\frac{\pi}{4} e_{13}} \\ &= e_1 + \frac{2}{s^2 + 1}\left(-s_1 e_3 + s_2 e_2 - e_1\right) \end{aligned} \tag{54}$$

and then down-project into the plane.

$$\begin{aligned} z &= \frac{e_3 \left(e_3 \wedge p_z\right)}{1 - e_3 \cdot p_z} \\ &= \frac{1}{1 - \frac{2 s_1}{s^2 + 1}}\left(e_1 + \frac{2}{s^2 + 1}\left(s_2 e_2 - e_1\right)\right) \end{aligned} \tag{55}$$

Which after some tedious simplifications produces,

$$z = \frac{1 + s}{1 - s}, \tag{56}$$

This article has been accepted for publication in a future issue of this journal, but has not been fully edited. Content may change prior to final publication. Citation information: DOI 10.1109/ACCESS.2017.2727819, IEEE Access



proving the hypothesis. The rotor which rotates the $s$ into $z$ is defined as

$$R_{zs} \equiv e^{-\frac{\pi}{4}e_{13}}. \tag{57}$$

The inverse transformation from impedance to reflection coefficient can be found by reversing the rotation orientation,

$$R_{sz} = \tilde{R_{zs}} = e^{\frac{\pi}{4}e_{13}}. \tag{58}$$

The subscript ordering makes sense when the rotors are used in the sandwich formula.

$$p_z = R_{zs}p_s\tilde{R_{zs}} = R_{zs}p_sR_{sz} \tag{59}$$

Once the original point $p_s$ is transformed into impedance $p_z$, the plane is re-interpreted as the Z-plane.

### B. Z-to-Y

In the complex domain, impedance and admittance values are related by complex inversion.

$$\mathbf{y} = \mathbf{z^{-1}} \tag{60}$$

Complex inversion is a widely used transform, so it is well known that it can be achieved through rotation of the Riemann sphere by $180°$ about the real axis [17]. Again, this can be deduced by up-projecting the points $\pm j, 0$, and $\infty$ onto the sphere and noticing how they move after an inversion, or through a proof similar to the last section. However, since this transform is well known it suffices to simply express it in rotor form. As described in Section II-F, complex inversion is equivalent to vector inversion followed by reflection in the hyperplane normal to $e_2$,

$$p_y = e_2e_3p_ze_3e_2. \tag{61}$$

Since two reflections produce a rotation, this can be expressed a $180°$ rotation in the $e_{23}$-plane (analogous to a rotation about the real-axis),

$$R_{zy} \equiv e_2e_3 = e^{-\frac{\pi}{2}e_{23}}. \tag{62}$$

Because the rotation is through $180°$, the inverse is itself.

$$R_{zy} = R_{yz} \tag{63}$$

### C. S-to-Y

The remaining transform between admittance and reflection coefficient can be found by combining the previous two. The result must be a rotation because it is a combination of two rotations.

$$\begin{aligned} R_{sy} = R_{sz}R_{zy} &= e^{\frac{\pi}{4}e_{13}}e^{-\frac{\pi}{2}e_{23}} \\ &= \frac{\sqrt{2}}{2}(1+e_{13})e_{23} \\ &= e^{-\frac{\pi}{2\sqrt{2}}(e_{23}+e_{21})} \end{aligned} \tag{64}$$

In three dimensions, taking the dual of the bivector argument gives the axis of the rotation.

$$(e_{23}+e_{21})\,e_{123} = -e_1+e_3 \tag{65}$$

Which demonstrates that this is a rotation about the $(e_3-e_1)$-axis. The relationships between the different circuit representations are illustrated by the graph in Figure 12.

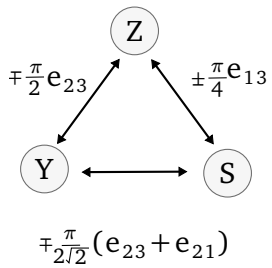


Figure 12: Graph representing of transformations relating different domains. Each path is labeled with the respective bivector.

### D. Summary

To summarize, Table I lists the various basis transformations and their generating bivectors, otherwise known as generators. Each is compared to the equivalent expression in complex algebra.

| Relation | Generator | Complex Algebra |
|---|---|---|
| Z2S | $\frac{\pi}{4}e_{13}$ | $\frac{\mathbf{z}-1}{\mathbf{z}+1}$ |
| S2Z | $-\frac{\pi}{4}e_{13}$ | $\frac{1+\mathbf{s}}{1-\mathbf{s}}$ |
| Z2Y | $-\frac{\pi}{2}e_{23}$ | $\frac{1}{\mathbf{z}}$ |
| Y2Z | $-\frac{\pi}{2}e_{23}$ | $\frac{1}{\mathbf{y}}$ |
| S2Y | $\frac{\pi}{2\sqrt{2}}(e_{23}+e_{21})$ | $\frac{1+\mathbf{s}}{1-\mathbf{s}}$ |
| Y2S | $-\frac{\pi}{2\sqrt{2}}(e_{23}+e_{21})$ | $\frac{1-\mathbf{y}}{1+\mathbf{y}}$ |

Table I: Basis transformations, their associated generating bivectors, and complex algebra equivalents.

### E. Alternative Perspectives

The Riemann Sphere model presented above leaves the projection point and plane stationary throughout the analysis, while the projected point $p$ is rotated about the sphere. In doing so, it forces one to re-interpret the projection plane each time a basis transformation is employed. A geometrical interpretation of this *extrinsic* interpretation is illustrated in Figure 13a. An alternative model is to fix a given circuit's position on the sphere and use different projection points and planes when translating into different 2D sub-spaces. This construction has the advantage that a physical circuit has a unique position on the sphere, and can be simultaneously projected into all domains, as illustrated in Figure 13b, and 14. The three different projection points are labeled as points of infinity in their respective domain. In contrast to the *extri*nsic model, the later interpretation may be called *intrinsic* model.

This article has been accepted for publication in a future issue of this journal, but has not been fully edited. Content may change prior to final publication. Citation information: DOI 10.1109/ACCESS.2017.2727819, IEEE Access



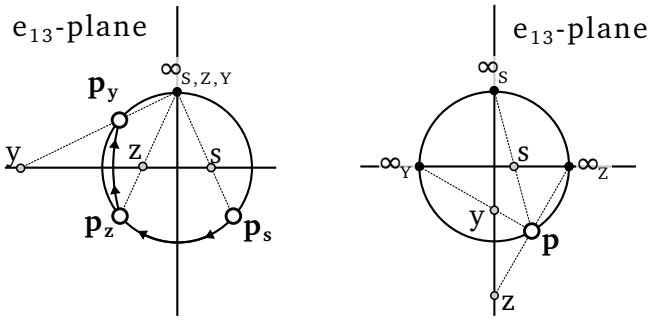


(a) *Extrinsic* model of the Riemann Sphere, as seen projected onto the $e_{13}$-plane. The second rotation from $p_z \rightarrow p_y$ is about the horizontal axis.

(b) *Intrinsic* model of the Riemann Sphere, as seen projected onto the $e_{13}$-plane.

Figure 13: Intrinsic and Extrinsic models for the Riemann Sphere.

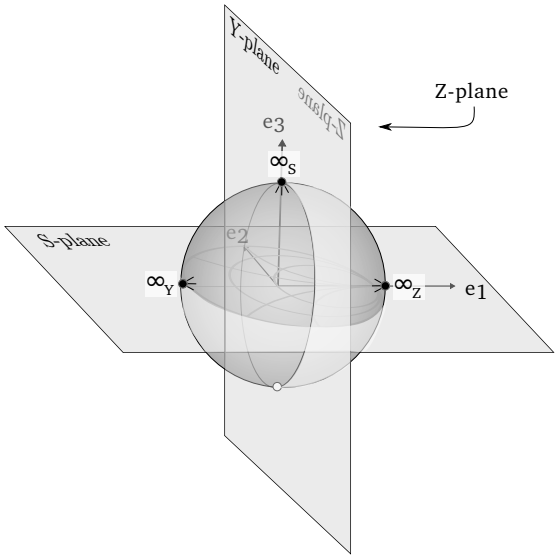


Figure 14: *Intrinsic* model of the Riemann Sphere in 3-dimensions.

The terms *extrinsic/intrinsic* are borrowed from a the subject of Euler angles, in which a similar dichotomy exists.

Using the intrinsic model, the different circuit representations can be seen as different basis sets, related by rotations. Any problem should be invariant to the basis that is chosen to frame it, and projective geometry provides this invariance. The basis rotors found above may be for either the intrinsic or extrinsic model. In the *extrinsic* model, the rotors act on the projected points laying on the sphere. In the *intrinsic* model the reversed rotors act on the projection point and plane. The bivectors must be reversed with translating between the intrinsic and extrinsic interpretations because the basis frame must rotate in an opposite orientation as points on the sphere. In the interest of simplicity and backward compatibility, we stick to the extrinsic model for the following analysis, but knowing that other perspective exist is useful.

## V. Applications

### A. Basic Use of Domain Transforms

To demonstrate usage of the basis rotors, an ideal short with impedance $z = 0$, is transformed from the impedance domain into the reflection coefficient domain. First, up-projecting $0$ onto the sphere,

$$p_z = \uparrow(0) = -e_3. \tag{66}$$

Then rotate into the reflection coefficient domain,

$$\begin{aligned} p_s &= R_{sz} e_3 R_{zs} \\ &= \frac{1}{2} e^{\frac{\pi}{4} e_{13}} (e_3)\, e^{-\frac{\pi}{4} e_{13}} \\ &= -e_1. \end{aligned} \tag{67}$$

Then down project into the plane

$$s = \downarrow(p_s) = \downarrow(-e_1) = -e_1. \tag{68}$$

Which is the expected result. Obviously, for this trivial example the overhead of projecting up and down outweighs any efficiency gained from linearizion. However, once the projective space becomes familiar there is no need start in 2D or down-project a result. For numerical applications up or down projecting are unnecessary unless the input or output of a given calculation is required to be translated.

### B. Input Impedance of a Transmission line

In this section we demonstrate how the domain rotors can also be used to transform circuit operators. Specifically, the effect of a matched transmission line is rotated from the reflection coefficient domain to the impedance domain. Interpreting the original $e_{12}$-plane as a reflection coefficient, the action of cascading a matched transmission line of length $\theta$ in front of the load performs a rotation of $-2\theta$ degrees in the plane, which may be written

$$p' = e^{\theta e_{12}} p e^{-\theta e_{12}}. \tag{69}$$

For brevity, define the matched line operator acting on s-parameters to be

$$L_s = L_s(\theta) \equiv e^{\theta e_{12}}. \tag{70}$$

Any functional dependence on arguments, ie $L(\theta)$, is be dropped unless relevant to the problem. For this section, and this section only, the operator subscripts $s$, $z$, and $y$ are used to denote the basis of an operator. In future sections, the functional invariance provided by CGA makes switching domains unnecessary and operator subscript are used for other purposes.

Given the operator for a matched transmission line in reflection coefficient domain, the equivalent operator in the impedance domain can be found by employing the basis rotors on the input and output quantities. This is done in three steps; first, transform the input quantity from impedance to reflection coefficient, apply the known $L_s$ operator, and then

This article has been accepted for publication in a future issue of this journal, but has not been fully edited. Content may change prior to final publication. Citation information: DOI 10.1109/ACCESS.2017.2727819, IEEE Access



transform back to impedance. The mapping is depicted in the commutative diagram shown in Figure 15.

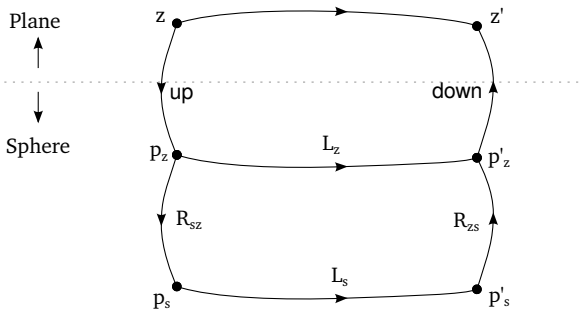


Figure 15: Commutative diagram illustrating how operators are transformed between different basis.

To illustrate, the computational flow is described step-by-step.

1) Take the original impedance vector $z$ and project it onto the sphere yielding $p_z$.

$$p_z = \uparrow(z) \tag{71}$$

2) Transform to s-parameters with the basis rotation.

$$p_s = R_{sz} p_z R_{zs} \tag{72}$$

3) Apply the matched transmission line operator $L_s$,

$$p'_s = L_s p_s \tilde{L_s}. \tag{73}$$

4) Transform back to impedance space.

$$p'_z = R_{zs} p'_s R_{sz} \tag{74}$$

Since all of these operators are rotations, the composite effect is also a rotation. To determine the net result, the series of operations may be written in a single expression,

$$p'_z = \underbrace{R_{zs} \overbrace{L_s \underbrace{R_{sz} p_z R_{zs}}_{\text{Z2S}} \tilde{L_s}}^{\text{apply line}} R_{sz}}_{\text{S2Z}}. \tag{75}$$

Using the properties of reversion, equation (75) may be re-written as,

$$p'_z = (R_{zs} L_s R_{sz})\, p_z\, (R_{zs} L_s R_{sz})^{\sim}. \tag{76}$$

Which gives the relationship between the matched line operator in the impedance and reflection coefficient,

$$L_z = R_{zs} L_s R_{sz}. \tag{77}$$

Thus, circuit operators are transformed into different representations just like circuit quantities, a property known as *covariance* [9]. This is a major conceptual and computational advantage of using geometric algebra for projective geometry. To determine $L_z$ the rotors are expanded and simplified,

$$\begin{aligned} L_z &= R_{zs} L_s R_{sz} \\ &= e^{-\frac{\pi}{4} e_{13}} e^{\theta e_{12}} e^{\frac{\pi}{4} e_{13}} \\ &= \cos(\theta) + \frac{1}{2}(1 - e_{13}) \sin\theta e_{12} (1 + e_{13}) \\ &= \cos(\theta) - \sin\theta e_{23} \\ &= e^{-\theta e_{23}}. \end{aligned} \tag{78}$$

The effect of a series transmission line in the impedance domain is a rotation in the $e_{23}$-plane. Interpreting the result geometrically, it is obvious that rotating the $e_{12}$-plane by $90^\circ$ about the $e_2$-axis produces $e_{23}$, so the proof is not really neccesary. Note that when $\theta = \frac{\pi}{2}$, a series transmission line is equivalent to the basis transformation between impedance and admittance. The matched line operator can be translated into admittance similarly,

$$\begin{aligned} L_y(\theta) &= R_{yz} L_z(\theta) R_{zy} \\ &= e^{\frac{\pi}{2} e_{23}} e^{-\theta e_{23}} e^{-\frac{\pi}{2} e_{23}} \\ &= e^{-\theta e_{23}} \\ &= L_z(\theta). \end{aligned} \tag{79}$$

This shows that a matched transmission line effects impedance and admittance in an identical way. By combining the Riemann sphere with the power of rotors, expressions provided by the conventional two-dimensional theory are substantially simplified. Additionally, the functional form of the circuit is not dependent on the domain in which it is interpreted, which removes the need to constantly switch domains within a single problem. In other words, the framework is domain-invariant. A comparison of the matched transmission line bivectors and their corresponding formula in the conventional two-dimensional theory is shown in Table II.

| Domain | Generator | Complex Algebra |
|---|---|---|
| s | $\theta e_{12}$ | $e^{-2\theta j}\mathbf{s}$ |
| z | $-\theta e_{23}$ | $\frac{\mathbf{z}+j\tan(\theta)}{1+\mathbf{z}j\tan(\theta)}$ |
| y | $-\theta e_{23}$ | $\frac{\mathbf{y}+j\tan(\theta)}{1+\mathbf{y}j\tan(\theta)}$ |

Table II: Comparison of the generators representing a matched transmission line compared to their complex algebra equivalents.

### C. Problems, and The Need For Another Dimension

It has been shown that by employing the Riemann sphere, the three major circuit representations may be related through rotations, producing a geometrical relationship between impedance, admittance and reflection coefficient. Additionally, the start of an operator-based approach to circuit theory has been demonstrated by mapping the effects of a matched transmission line onto the sphere and rotating it into the impedance domain. Throughout the developments, geometric algebra provides the necessary machinery to efficiently discuss these geometric concepts algebraically.

This article has been accepted for publication in a future issue of this journal, but has not been fully edited. Content may change prior to final publication. Citation information: DOI 10.1109/ACCESS.2017.2727819, IEEE Access



While the developments thus far are not without benefit, the system is missing several important features required for practical usage. Rotations and domain transformations are linearized but common operations such as addition and scaling are awkward to accomplish on the sphere. The solution to this problem is to add an additional dimension of negative signature, producing a geometry that is known as Conformal Geometric Algebra (CGA) [8]. The relationship between the geometric algebras used for the Smith Chart, Riemann Sphere, and Conformal models are illustrated below.

$$\underbrace{\mathbb{C} \Longrightarrow G_2}_{\text{Smith Chart}} \longrightarrow \underbrace{G_3}_{\text{Riemann Sphere}} \longrightarrow \underbrace{G_{3,1}}_{\text{CGA}} \tag{80}$$

All of the basis transformations, and transmission line rotors developed on the Riemann sphere are directly re-usable in the CGA framework, so no work is lost by moving into CGA.

## VI. Conformal Geometric Algebra and Transmission Line Theory

A full introduction to CGA is out of the scope of this paper. However, the fundamentals of CGA have been sufficiently explained by numerous other authors [8], [9], [15], [18], and we direct the unacquainted to these resources. Our introduction of CGA by way of stereographic projection is similar to that given in [8].

### A. Mappings

As with stereographic projection, the purpose of CGA is to map vectors into a space of higher dimension to simplify certain operations. For our purposes, CGA is used to convert Möbius transformations into rotations. Building off the stereographic projection model, a vector in a plane is mapped onto a point on the Riemann Sphere by,

$$p = \left(\frac{x^2-1}{x^2+1}\right) e_3 + \left(\frac{2}{x^2+1}\right) x. \tag{81}$$

Add to this a new dimension of negative signature represented by the vector $e_4$, producing a four-dimensional vector $X$.

$$X = \left(\frac{x^2-1}{x^2+1}\right) e_3 + \left(\frac{2}{x^2+1}\right) x + e_4 \tag{82}$$

Because $e_4^2 = -1$ the vector $X$ is null, meaning $X^2 = 0$. Therefore, $X$ and $\lambda X$ represent the same point, a property known as homogeneity. Exploiting this property, $X$ can be simplified by multiply by $\left(x^2+1\right)$ yielding,

$$X = \left(x^2-1\right) e_3 + 2x + \left(x^2+1\right) e_4. \tag{83}$$

At this point we have an orthonormal vector basis,

$$e_1^2 = e_2^2 = e_3^2 = -e_4^2 = 1. \tag{84}$$

Those familiar with relativity will recognize this geometry as that of space-time. The basis generates a geometric algebra containing the following blades.

$$\underbrace{\alpha}_{1-\text{scalar}}, \underbrace{e_i}_{4\text{-vectors}}, \underbrace{e_{ij}}_{6-\text{bivectors}}, \underbrace{e_{ijk}}_{4\text{-trivectors}}, \underbrace{I}_{1\text{-pseudoscalar}} \tag{85}$$

Here the $e_{12}$-plane is identified as the original 2D space, and $e_{34}$-plane contains the added dimensions. A consequence of the vector basis having a mixed signature is that any bivector containing $e_4$ will have a positive square. This expands the concept of rotations to include hyperbolic rotations. Applying Euler's identity with a bivector of positive square yields,

$$e^{\theta e_{14}} = \cosh + \sinh \theta. \tag{86}$$

The $e_{34}$-plane plays a special role and is known as the *Minkowski plane,* commonly labeled $E_0$,

$$E_0 \equiv e_3 \wedge e_4. \tag{87}$$

It is convenient to further define a *null* basis.

$$e_o = \frac{1}{2}\left(e_4 - e_3\right) \tag{88}$$

$$e_\infty = e_4 + e_3 \tag{89}$$

These two vectors represent the points of infinity and zero, as their subscripts suggest. They have the properties,

$$e_o^2 = e_\infty^2 = 0 \tag{90}$$

$$e_\infty e_o = -1 + E_0. \tag{91}$$

In terms of the null basis, a vector $x$ in the original space of $e_{12}$ is mapped *upwards* to a conformal vector $X$, by the following.

$$X = \uparrow(x) = x + \frac{1}{2}x^2 e_\infty + e_o \tag{92}$$

The inverse, *downwards* map, is the made by normalizing the conformal vector then rejecting it from the Minkowski plane.

$$x = \downarrow(X) = \frac{X \wedge E_0}{-X \cdot e_\infty} E_0^{-1} \tag{93}$$

In the above formula and all others, we adhere to the convention that the inner and outer products take precedence over the geometric product. Rotations in different planes within the CGA space implement various operations in the original space that are non-linear, such as translation and involution (negation). Both rotation and reflection operators follow similar forms, and are referred to as *versors* in CGA. Reviewing some common results from the literature [8], a list of CGA operators which we will make use of are provided in Table III along with their complex equivalents.

| Operation | Complex Function | CGA Versor |
|---|---|---|
| Translation | $\mathbf{z}+a$ | $e^{\frac{1}{2}e_\infty a}$ |
| Rotation | $e^{\theta j}\mathbf{z}$ | $e^{-\frac{1}{2}\theta e_{12}}$ |
| Dilation | $\lambda\mathbf{z}$ | $e^{-\frac{1}{2}\ln\lambda E_0}$ |
| Vector Inversion | $\left(\mathbf{z}^\dagger\right)^{-\mathbf{1}}$ | $e_3$ |
| Complex Inversion | $\mathbf{z}^{-\mathbf{1}}$ | $e_{23}$ |
| Involution | $-\mathbf{z}$ | $E_0$ |
| Reflection | uncommon | $a$ |

Table III: Common versors used in CGA, and their complex equivalent.

### B. Addition of Impedance and Admittance

The difficulty of implementing addition on Riemann Sphere is remedied with the use of CGA as we will now show. The additional of a series impedance is modeled as a translation in the impedance domain. In CGA, a translation by the vector $z$ is achieved with a rotation in the $e_\infty \wedge z$ plane.

$$T_z = 1 + \frac{1}{2}e_\infty z \tag{94}$$

To determine the equivalent operator in the s-domain, the operator is rotated by the appropriate basis transformation.

$$R_z = R_{sz}T_zR_{zs} \tag{95}$$

Because it is physically meaningful to distinguish resistance and reactance, we solve for translation in each component independently. Of course, the results can be combined to handle arbitrary impedances. Interpreting the $e_1$ direction as resistance, the effect of adding a normalized resistance of amount $r$ is produced by,

$$T_r = 1 + \frac{r}{2}e_\infty e_1 = e^{\frac{r}{2}e_\infty e_1}. \tag{96}$$

Computing the resultant rotation in the s-domain.

$$\begin{aligned} R_r &= e^{\frac{\pi}{4}e_{13}}e^{\frac{1}{2}e_\infty re_1}e^{-\frac{\pi}{4}e_{13}} \\ &= \frac{1}{2}(1+e_{13})(1+\frac{1}{2}re_{31}+\frac{1}{2}re_{41})(1-e_{13}) \\ &= 1+\frac{r}{2}e_3(e_4+e_1) \\ &= e^{\frac{r}{2}(e_{34}-e_{13})} \end{aligned} \tag{97}$$

Modeling the addition of a normalized reactance $x$ by a translation in $e_2$, the reactance rotor is found,

$$\begin{aligned} R_x &= e^{\frac{\pi}{4}e_{13}}e^{\frac{1}{2}e_\infty xe_2}e^{-\frac{\pi}{4}e_{13}} \\ &= e^{\frac{x}{2}(e_{12}-e_{24})}. \end{aligned} \tag{98}$$

A similar analysis yields the rotor for adding conductance and susceptance.

$$\begin{aligned} R_g &= R_{sy}T_gR_{ys} \\ &= e^{-\frac{\pi}{2\sqrt{2}}(e_{23}+e_{21})}e^{\frac{1}{2}e_\infty ge_1}e^{\frac{\pi}{2\sqrt{2}}(e_{23}+e_{21})} \\ &= e^{\frac{g}{2}(e_{34}+e_{13})} \end{aligned} \tag{99}$$

$$\begin{aligned} R_b &= R_{sy}T_bR_{ys} \\ &= e^{-\frac{\pi}{2\sqrt{2}}(e_{23}+e_{21})}e^{\frac{1}{2}e_\infty be_2}e^{\frac{\pi}{2\sqrt{2}}(e_{23}+e_{21})} \\ &= e^{\frac{b}{2}(e_{12}+e_{24})} \end{aligned} \tag{100}$$

The rotors $R_r$ and $R_x$ will rotate a load about circles of constant reactance and resistance, while $R_g$ and $R_b$ will rotate a load about circles of constant susceptance and conductance, respectively. The effects of each rotor as seen on the reflection coefficient plane are shown in Figure (16). These rotors sweep out the familiar impedance and admittance contours of the Smith Chart. However, because these rotations are non-euclidean they cannot be succinctly represented within complex algebra. Instead, one has to cascade three individual operations: transform to impedance, translate, transform to reflection coefficient. This difficulty is one reason the Smith Chart is used as a nomogram.

### C. Bivector Algebra and Discrete Element Group

One advantage of using geometric algebra is that it exposes the group structure underlying the transformations [19]. Identifying the bivectors for the impedance/admittance rotors found above.

$$R \equiv e_{34} - e_{13} \tag{100a}$$
$$X \equiv e_{12} - e_{24} \tag{100b}$$
$$G \equiv e_{34} + e_{13} \tag{100c}$$
$$B \equiv e_{12} + e_{24} \tag{100d}$$

A bivector group can be found by employing all combinations of the commutator product, defined by

$$A \times B \equiv \frac{1}{2}\left(AB - BA\right), \tag{101}$$

to the bivectors $R, X, G$ and $B$. When this is done, two new bivectors are found.

$$N \equiv e_{14} \tag{102}$$
$$Q \equiv -e_{23} \tag{103}$$

The rotors which make use of these bivectors are defined,

$$R_n \equiv e^{-\ln(n)e_{14}} \tag{104}$$
$$R_q \equiv e^{qe_{23}}. \tag{105}$$

To determine what operations these bivectors represent, an arbitrary load can be rotated in the bivector planes of $N$ and $Q$, while recording its path on the 2D reflection coefficient plane. Doing so generates the contours shown in Figure (17), which

This article has been accepted for publication in a future issue of this journal, but has not been fully edited. Content may change prior to final publication. Citation information: DOI 10.1109/ACCESS.2017.2727819, IEEE Access



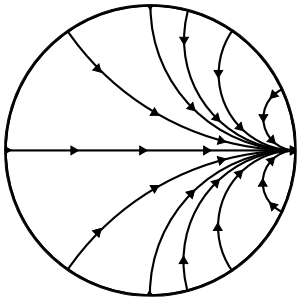

(a) Rotation in $R \equiv e_{34} - e_{31}$.

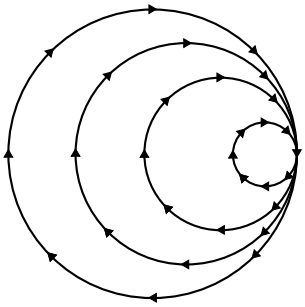

(b) Rotation in $X \equiv e_{12} - e_{24}$

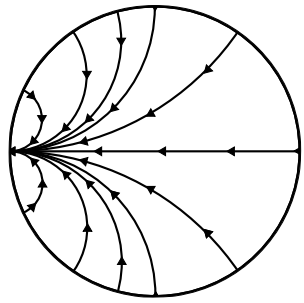

(c) Rotation in $G \equiv e_{34} + e_{13}$

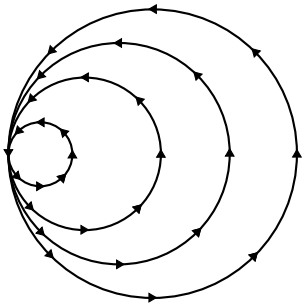

(d) Rotation in $B \equiv e_{12} + e_{24}$

Figure 16: Effects of Rotations in bivectors $R, X, G$, and $B$.

| | $R$ | $X$ | $G$ | $B$ | $N$ | $Q$ |
|---|---|---|---|---|---|---|
| $R$ | 0 | | | | | |
| $X$ | 0 | 0 | | | | |
| $G$ | $2N$ | $-2Q$ | 0 | | | |
| $B$ | $-2Q$ | $-2N$ | 0 | 0 | | |
| $N$ | $-R$ | $-X$ | $G$ | $B$ | 0 | |
| $Q$ | $X$ | $-R$ | $-B$ | $-G$ | 0 | 0 |

Table IV: Commutator table for discrete circuit bivector group.

are recognized as contours of the *Carter Chart [1]* ( known in other fields as a Wulff Net). These contours correspond a change in characteristic impedance magnitude and phase components. This can be proven by rotating the bivectors into the impedance domain, and ensuring they correspond to dilation and rotation generators. First, transform $N$.

$$R_{zs} N R_{sz} = e^{\frac{-\pi}{4} e_{13}} e_{14} e^{\frac{\pi}{4} e_{13}} = e_{34} \tag{106}$$

Which is the bivector that generates dilations, while

$$R_{zs} Q R_{sz} = -e^{\frac{-\pi}{4} e_{13}} e_{23} e^{\frac{\pi}{4} e_{13}} = e_{12}. \tag{107}$$

Which is the bivector that generates rotations in the original 2D space. The Carter Chart is a polar coordinate system in impedance domain that has been transformed into the reflection coefficient domain. Explicitly defining the operators for changing characteristic impedance is useful for analyzing transmission line dynamics, as demonstrated in the next section.

The Smith Chart with impedance and admittance contours combined with the Carter Chart represent paths formed from the rotors of a bivector group. This group contains elements of impedance, admittance, and characteristic impedance change, and so it might be referred to as the *discrete element* group. Table (IV) provides the commutator relations which define the group. Identifying circuit elements as a bivector group has many important consequences. All of the equivalent circuit relationships, duality properties, and infinitesimal behaviors can be derived from properties of the group.

The pairs of bivectors used to generate each chart are orthogonal.

$$R \cdot X = G \cdot B = Q \cdot N = 0 \tag{108}$$

So that pairs commute, as one would expect. Each pair is also inter-related by duality.

$$RI = X \tag{109}$$
$$GI = B \tag{110}$$
$$QI = N \tag{111}$$

This article has been accepted for publication in a future issue of this journal, but has not been fully edited. Content may change prior to final publication. Citation information: DOI 10.1109/ACCESS.2017.2727819, IEEE Access



Which shows there is a complex structure within the bivector algebra, as expressed by the equations.

$$Z = rR + xX = (r + xI)R \tag{112}$$
$$Y = gG + bB = (g + bI)\,G \tag{113}$$
$$P = qQ + nN = (q + nI)\,Q \tag{114}$$

The pairs can also be related to one another through the operation of reflection in the hyperplane normal to $e_4$, analogous to *time-reversal* in Space-Time Algebra [20].

$$\bar{x} \equiv e_4 x e_4 \tag{115}$$

This produces the relationships.

$$\bar{R} = G \tag{116}$$
$$\bar{X} = B \tag{117}$$
$$\bar{N} = N \tag{118}$$
$$\bar{Q} = -Q \tag{119}$$

All of the bivectors are *simple*, meaning they square to a scalar. Classifying the bivectors based on the sign of their square turns out to be useful. Borrowing some terminology from Space-Time Algebra, it may be said that $R, X, G$ and $B$ are *light-like*, $N$ is *space-like*, and $Q$ is *time-like*, meaning,

$$R^2 = X^2 = G^2 = B^2 = 0 \tag{120}$$
$$N^2 = -Q^2 = 1. \tag{121}$$

Because the signature we have employed is opposite that used in Space-Time Algebra, our meaning of *space-like* and *time-like* is inverted.

## VII. Distributed Element Model

A fundamental part of transmission line theory is the distributed element model. In this model, a uniform transmission line is represented as an infinite sum of infinitesimal lumped elements cascaded together, a unit cell of which is shown in Figure (18). Normally the properties of transmission line are studied through differential equations relating voltages and currents along the lines, but we will examine the dynamics produced by this model through the CGA operator framework.

A unit cell of the distributed element model is composed of reactance $X$, resistance $R$, susceptance $B$, and conductance $G$. As shown in the previous section, the effect of each component in the distributed element model is a rotation in the conformal model. Therefore, to determine the effect of an infinitesimal element, we need to compute the effect of an infinitesimal rotation. Following the approach in [9], the rotation of a vector $a$ by a small bivector $\delta B$ may be written

$$e^{-\delta B} a e^{\delta B} = a + \delta a \times B + \delta^2 (...)\,. \tag{122}$$

Where $\times$ is the commutator product, and $\delta^2 (...)$ are higher order terms which disappear as $\delta$ becomes infinitely small. The subsequent rotation of another small bivector $C$ yields,

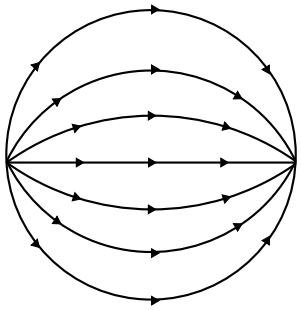

(a) Rotation in $N \equiv e_{14}$

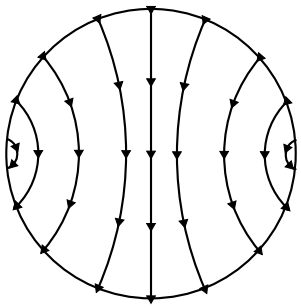

(b) Rotation in $Q = -e_{23}$.

Figure 17: Effects of Rotations in bivectors $N$ and $Q$. The contours are that of the Carter Chart.

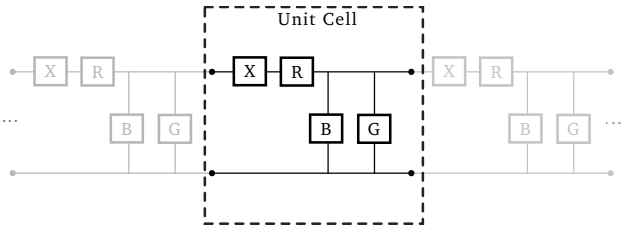


Figure 18: Distributed element model

$$e^{-\delta_c C} e^{-\delta_b B} a e^{\delta_b B} e^{\delta_c C} = a + a \times (\delta_b B + \delta_c C) + \delta^2 (...) \simeq e^{-(\delta_b B + \delta_c C)} a e^{(\delta_b B + \delta_c C)} \tag{123}$$

Illustrating that to first order, small rotations commute and the bivector of the rotation is simply the sum of their bivectors. Returning to the distributed element model, the total rotor for a single unit cell as depicted in Figure 18 is,

$$e^{\frac{x}{2} X} e^{\frac{r}{2} R} e^{\frac{b}{2} B} e^{\frac{g}{2} G} \tag{124}$$

Where $x, r, b$ and $g$ are scalars, and $X, R, B$, and $G$ are the bivectors given in section VI-C. In the limit that $x, r, b$ and $g$ become infinitely small, the rotor for a distributed element unit cell becomes

$$\lim_{x,r,g,b \to 0} e^{\frac{x}{2} X} e^{\frac{r}{2} R} e^{\frac{b}{2} B} e^{\frac{g}{2} G} \simeq e^{\frac{1}{2}(xX + rR + bB + gG)}. \tag{125}$$

Once the limit is taken, the values of $x, r, b$ and $g$ become *distributed*, meaning they have units inversely proportional to distance. The rotor for a section of line of length $l$, is therefore

This article has been accepted for publication in a future issue of this journal, but has not been fully edited. Content may change prior to final publication. Citation information: DOI 10.1109/ACCESS.2017.2727819, IEEE Access



$$R_{xrbg} \equiv e^{\frac{l}{2}(xX+rR+bB+gG)}. \tag{126}$$

Expanding the generator and grouping like terms yields,

$$R_{xrbg} = \frac{l}{2}\left((x+b)\,e_{12} + (x-b)\,e_{24} + (g+r)\,e_{34} + (g-r)\,e_{13}\right). \tag{127}$$

This bivector contains all of the physics of a distributed element transmission line. It produces bivectors which are outside of the discrete element group. The $e_{12}$ and $e_{34}$ components are recognized as euclidean rotations and dilations, respectively. Anticipating the importance of these bivectors in the analysis to follow, assign variables and make note of their properties.

$$L \equiv e_{12} \tag{128}$$

$$A \equiv e_{34} \tag{129}$$

They are orthogonal,

$$L \cdot A = 0, \tag{130}$$

dual to one-another,

$$AI = L, \tag{131}$$

and affected by time-reversal with

$$\bar{A} = A \tag{132}$$

$$\bar{L} = -L. \tag{133}$$

Additionally, $L$ is *time-like*, and $A$ is *space-like*. The rotors which employ these bivectors can be defined,

$$\begin{aligned} R_l &\equiv e^{\theta e_{12}} \\ R_a &\equiv e^{-\frac{1}{2}\ln(\alpha)e_{34}}. \end{aligned}$$

While the subscripts $l$ and $a$ do not match the scalar arguments of the rotor, they do match bivector variables and the description for the circuits which produce them, i.e. a *line* and *attenuator.* To explore the effects of the various bivector components in eq (127), we examine a few special cases of a the distributed element transmission line model.

### A. Lossless

In the case of a lossless line the resistance and conductance are zero, $g = r = 0$. In this case we are left with rotations in both $e_{12}$ and $e_{24}$ in amounts that depend on the difference between $b$ and $x$. The nature of these rotations can best understood by visualizing their effect on the Smith Chart, as shown in Figure 19. When $\frac{b}{x} = 1$, the distributed element bivector reduces to $e_{12}$. This produces a euclidean rotation of the reflection coefficient centered at 0, shown in Figure 19b. Rotations of this type are expected from an ideal lossless transmission line, and produce paths known as *Standing Wave Ratio (SWR)* Circles. Depending on the signs of $b$ and $x$, either clockwise or counterclockwise rotations are produced. These two scenarios depict right-handed, and left-handed transmission lines.

In the case where the normalized susceptance is larger that the reactance, $\frac{b}{x} > 1$, the rotation shown in 19a is produced. This is a non-euclidean rotation centered about the normalized characteristic impedance of the line, a fact proved later in this section. A transmission line of this type is more *susceptive* than the reference impedance. The term more *susceptive* generally implies more capacitive, but this requires a sign choice for $b$ which we choose not to make at this point. Leaving the sign ambiguous allows for artificial transmission lines. In either case, the sign only changes the direction of the rotation, so its a minor difference to the geometry. The final case, $\frac{b}{x} < 1$, is similar to the susceptive case, but is more reactive rather than susceptive.

In the extremes that $\frac{b}{x} \gg 1$ or $\frac{b}{x} \ll 1$,the generators reduce to $B$ and $X$, and produce the rotations shown in Figure 16. This makes sense, because summing a series of mostly reactance elements is equivalent to a lumped reactance and likewise for susceptance. Reflecting on Figure 19, we see there is a smooth transition between: pure susceptance, a susceptive line, a matched line, a reactive line, and pure reactance.

### B. Non-propagating

Before examining lossy lines, it helpful to look at the effects of non-propagating lines, i.e. $x = b = 0$ but $g \neq 0$ and/or $r \neq 0$, because they are dual to the lossless case. Looking at eq (127), these conditions will produce rotations in $e_{34}$ and $e_{13}$ in amounts depending on the ratios of $r$ and $g$. Proceeding in a similar way as with the lossless lines, the contours created by such rotations are plotted on the Smith Chart in Figure 20. In the extremes that $\frac{g}{r} \gg 1$ or $\frac{g}{r} \ll 1$, the rotation bivectors reduce to $G$ and $R$, as shown in Figure 16. Analogous to the lossless cases, there is a smooth transition between: pure conductance, a conductive attenuator, a matched attenuator, a resistive attenuator, and pure resistance.

### C. Lossy

In the general case of lossy lines several different rotations can be produced. In general they are all spirals, which center about the characteristic impedance. We examine a few cases of lossy lines in Figure 21. When $\frac{b}{x} = \frac{r}{g} = 1$, the line is matched, and this results in a rotation centered about the center of the Smith Chart as shown in Figure 21b. The bivector contains only components in $e_{12}$ and $e_{34}$, which are recognized as euclidean rotation and scaling operators. As the line becomes more conductive $\frac{g}{r} > 1$, the characteristic impedance moves downwards and to the right. And when the line becomes more resistive $\frac{g}{r} < 1$, the characteristic impedance moves upwards and to the left.

While more work could be done to characterize the dynamics of different transmission lines, we move on to an alternative model for the same circuit which uses a matched/mismatched dichotomy instead of the distributed elements. By relating the two models components of the distributed element bivector are given physical meaning.

This article has been accepted for publication in a future issue of this journal, but has not been fully edited. Content may change prior to final publication. Citation information: DOI 10.1109/ACCESS.2017.2727819, IEEE Access



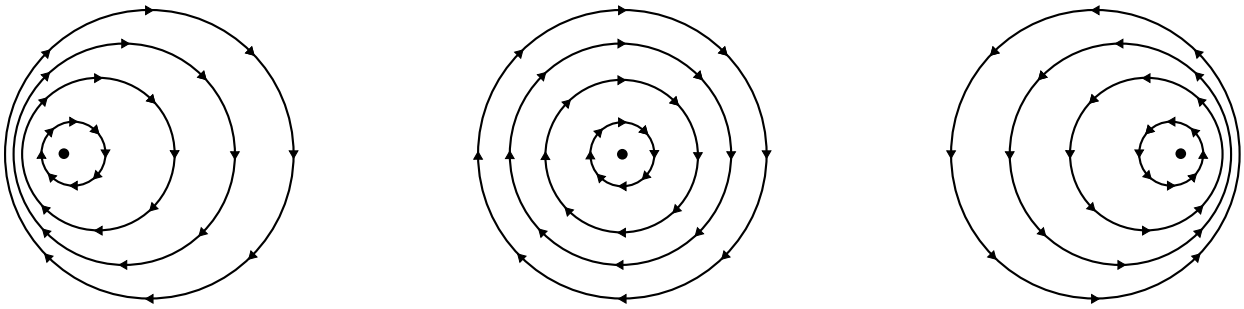

(a) Rotations with $\frac{b}{x} > 1$. (b) Rotations with $\frac{b}{x} = 1$ (c) Rotations with $\frac{b}{x} < 1$

Figure 19: Rotations produced by a lossless distributed element model, showing the effects of different ratios of distributed reactance and susceptance. The rotation direction (clockwise vs counterclockwise) changes depending on the signs of $b$ and $x$.

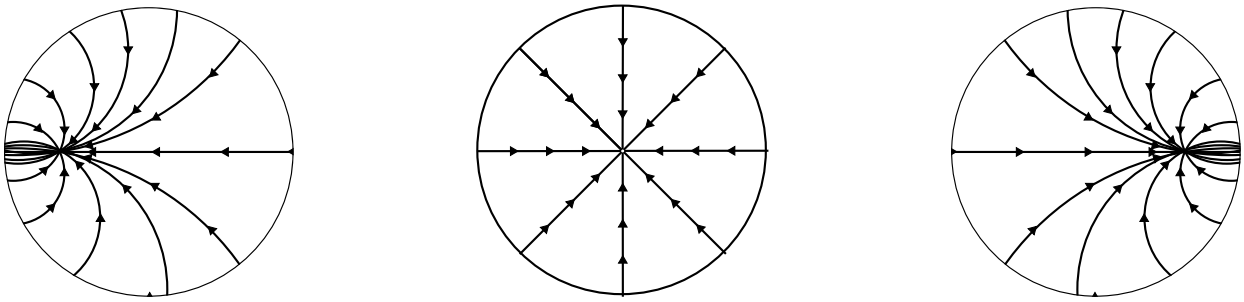

(a) Rotations with $\frac{g}{r} > 1$. (b) Rotations with $\frac{g}{r} = 1$ (c) Rotations with $\frac{g}{r} < 1$

Figure 20: Rotations produced by a distributed loss, showing the effects of different ratios of distributed resistance and conductance. The rotation direction (clockwise vs counterclockwise) changes depending on the signs of $g$ and $r$.

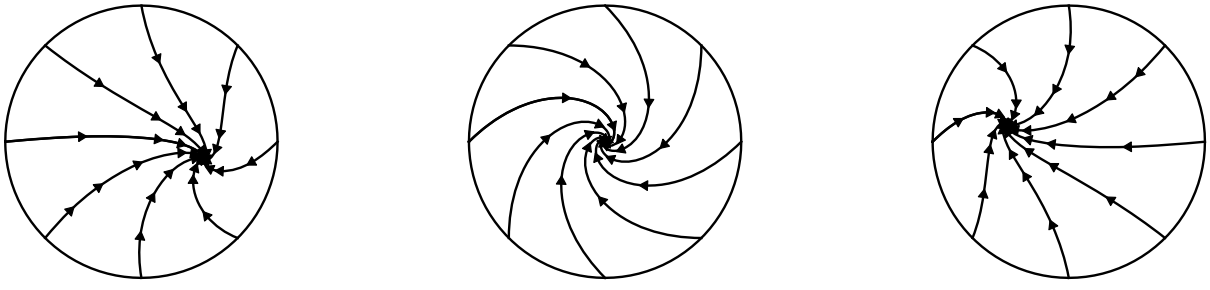

(a) Rotations with $\frac{b}{x} = 1, \frac{g}{r} > 1$. (b) Rotations with $\frac{b}{x} = 1, \frac{g}{r} = 1$ (c) Rotations with $\frac{b}{x} = 1, \frac{g}{r} < 1$

Figure 21: Rotations produced by lossy lines. The amount of loss is exaggerated from typical values to show the characteristics of the rotation.

This article has been accepted for publication in a future issue of this journal, but has not been fully edited. Content may change prior to final publication. Citation information: DOI 10.1109/ACCESS.2017.2727819, IEEE Access



### D. Relating the Distributed Element and Transformer Models

When $\frac{b}{x} \neq 1$ and/or $\frac{r}{g} \neq 1$, the distributed element model results in a mismatched transmission line. Another way to represent a mismatched transmission line is to sandwich a matched line in between two impedance steps of equal but inverse impedance changes. This may be referred to as the *transformer* model. An illustration of a mismatched transmission line realized in half-space, and the corresponding impedance step circuit model is shown in Figure 22. A change in line impedance can be modeled as a scaling and rotation in the impedance domain, operations which are implemented with $N$ and $Q$ bivectors as found earlier. It is most common to deal with changes in real characteristic impedance, which is equivalent to scaling, so we focus on effects of $N$ for now. The rotor used to scale an impedance by a factor of $n$, i.e. $z \to nz$ was found to be

$$R_n = e^{-\frac{1}{2}\ln(n)e_{14}}. \tag{134}$$

An impedance scaling of inverse amount $n \to \frac{1}{n}$, is equal to the reversed rotor,

$$e^{-\frac{1}{2}\ln(\frac{1}{n})e_{14}} = e^{\frac{1}{2}\ln(n)e_{14}} = \tilde{R_n} \tag{135}$$

Using this result, a lossless, mismatched transmission line may be represented in the *transformer* model as,

$$\tilde{R_n} R_l R_n = e^{\frac{1}{2}\ln(n)e_{14}} e^{\theta e_{12}} e^{-\frac{1}{2}\ln(n)e_{14}}. \tag{136}$$

This equation could be interpreted as *boosting* the $e_{12}$ plane, borrowing language from relativity. A relationship between the transformer and distributed element models must exist because they represent the same physical circuit. This knowledge allows us to equate the rotors for each model.

$$e^{\frac{l}{2}(xX+bB)} = e^{\frac{1}{2}\ln(n)e_{14}} e^{\theta e_{12}} e^{-\frac{1}{2}\ln(n)e_{14}} \tag{137}$$

Explicit relationship between these two parameterizations can be found by further equating their generators, which requires the bivector argument for the transformer model to be found. To do this, note that rotating a rotor is equivalent to rotating it's bivector argument [9].

$$Re^{B}\tilde{R} = e^{RB\tilde{R}} \tag{138}$$

Where $R$ is a rotor and $B$ is a bivector. This allows the transformer's generator to be found by,

$$\begin{aligned} R_n e_{12} \tilde{R_n} =& e^{\frac{1}{2}\ln(n)e_{14}} \theta e_{12} e^{-\frac{1}{2}\ln(n)e_{14}} \\ =& \theta\left(\cosh\left(\ln\left(n\right)\right)e_{12} + \sinh\left(\ln\left(n\right)\right)e_{24}\right). \end{aligned} \tag{139}$$

Which provides an interpretation for the $e_{24}$ component in the distributed element bivector as the result of mismatching a lossless line. Setting eq (139) equal to eq (127), produces the following relationships,

$$\frac{l}{2}(x+b) = \theta\cosh\left(\ln\left(n\right)\right) \tag{140}$$

$$\frac{l}{2}(x-b) = \theta\sinh\left(\ln\left(n\right)\right). \tag{141}$$

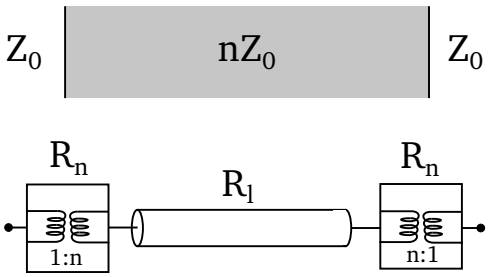


Figure 22: A lossless mismatched transmission line in half-space (above) and it's equivalent circuit model (below). The $R_n$-blocks represent impedance discontinuities, and the $R_L$ a matched line.

This pair of equations may be solved for the impedance scaling factor $n$ in terms of distributed elements.

$$n = \sqrt{\frac{x}{b}} \tag{142}$$

Similarly, the electrical length of the line can be found.

$$\theta = \frac{l}{2}\sqrt{xb} \tag{143}$$

Thus, the impedance scaling factor $n$ is the normalized characteristic impedance of the lossless transmission line between the impedance steps. This proves the earlier claim that the rotations shown in Figure 19 rotate about the line's characteristic impedance. To see this, note that eq (136) moves the impedance value $n$ to the origin, rotates by $\theta$, then moves the origin back to an impedance value of $n$. Therefore, the new center of rotation will be at an impedance of $n$. Computing where $R_n$ moves the center of the rotation can done explicitly.

$$\begin{aligned} \downarrow R_n e_o \tilde{R_n} =& \downarrow e^{-\frac{1}{2}\ln(n)e_{14}}\left(e_4 - e_3\right)e^{\frac{1}{2}\ln(n)e_{14}} \\ =& \downarrow \left(-e_3 + \cosh\left(\ln\left(n\right)\right)e_4 + \sinh\left(\ln\left(n\right)\right)e_1\right) \\ =& \tanh\left(\frac{1}{2}\ln\left(n\right)\right)e_1 \\ =& \frac{n-1}{n+1}e_1 \end{aligned} \tag{144}$$

Which is the reflection coefficient for an impedance value of $n$, as claimed.

### E. Units of Distributed Elements

The meaning of $b$ and $x$ as normalized quantities may appear strange given no characteristic impedance has been defined. In essence, if $b$ and $x$ are set to be equal, then we have implicitly defined the characteristic impedance. To see this, express $b$ and $x$ in terms of the characteristic impedance and admittance.

$$x = \frac{x'}{Z_0} \qquad b = \frac{b'}{Y_0} \tag{145}$$

Where $x'$ and $b'$ are the *un-normalized* values of distributed reactance and susceptance, respectively. By setting

$$\frac{x}{b} = 1. \tag{146}$$

We have implied

$$\frac{x'}{Z_0}\frac{Y_0}{b'} = 1$$
$$\frac{x'}{b'} = Z_0^2. \tag{147}$$

Which defines $Z_0$. Similarly the product of $xb$ in eq (143) defines the normalized propagation constant,

$$\sqrt{xb} = \sqrt{\frac{x'}{Z_0}\frac{b'}{Y_0}} = \frac{\gamma_l}{\gamma_0} \tag{148}$$

### *F. Systematic Method for Determining Equivalent Circuits of Mismatched Transmission Lines*

So far, two parameterizations for a specific class of mismatched transmission lines have been developed. Namely, the distributed element model containing reactance and susceptance has been related to a lossless transmission line mismatched by an impedance scaling. It is conjectured that the general case of a arbitrarily mismatched lossy line can be modeled as matched transmission line sandwiched in between two arbitrary impedance steps, given by,

$$\tilde{R_n}\tilde{R_q}R_lR_aR_qR_n. \tag{149}$$

This rotor has 4 degrees of freedom $(n, q, \theta, \alpha)$, which matches that of the distributed element model $(r, x, g, b)$, as required. The commutation relations of the bivectors allows the transformer model to be put into the more concise form,

$$\tilde{R_{nq}}R_{la}R_{nq}. \tag{150}$$

Where,

$$R_{la} = e^{\theta e_{12} - \ln(\alpha)e_{34}} \tag{151}$$
$$R_{nq} = e^{-(qe_{23} + \ln(n)e_{14})}. \tag{152}$$

The statement expressing the equivalence between the transformer model and the distributed element model is most concisely written.

$$\tilde{R_{nq}}R_{la}R_{nq} = R_{xrgb} \tag{153}$$

Given this expression, determining relationships between the two parameterizations reduces to equating the generators for each rotor, a procedure which can be done systematically. A thorough classification of transmission lines and the relationship between the transformer and distributed element model would be interesting to work out in the future.

### *G. Discussion*

The CGA operator framework has been used to derive the effects of distributed element transmission lines without differential equations. However, we are not suggesting the classic analysis of transmission lines by way of the telegrapher's equations should be forgone. Instead, our goal has been to demonstrate that the unique ability of CGA to handle non-euclidean rotations allows the physics of non-matched transmission lines to be more accurately expressed. The relationship between the distributed circuit and transformer models has been derived, and the characteristic impedance was shown to be a fixed point of the CGA rotations for lossless lines. It is interesting that the three specific classes of transmission lines correspond to the three classes of Möbius transformations [17]. The lossless lines are *elliptic*, the distributed loss lines are *hyperbolic*, and the lossy lines are *loxodromic*. This can be proved by an analysis of their fixed points. Additionally, because every Möbius transformation has two fixed points, every mismatched transmission line produces two characteristic impedances, one of which is active. Increasing the radius of the Smith Chart beyond unity allows both fixed points to be seen. While a fixed point analysis with CGA would be interesting, we instead move on to demonstrate an example application to impedance matching, and leave the fixed point analysis for future study.

## VIII. Impedance Matching

In this section the results derived thus far are applied to problems of impedance matching. Specifically, the topologies of single shunt stub tuner and the impedance transformer are solved. Both of these problems are approached with the same technique.

1) Determine the operator representation of the network
2) Invert the operator, to produce an equation for the unknown load
3) Solve for the rotor parameters.

By using CGA operators, all networks have similar functional forms regardless of their domain. Therefore, we choose to solve the problem entirely in terms of reflection coefficient (the s-domain), so that it can be visualized on the Smith Chart. The invertability of the verser product makes computing the solution straightforward, but does not grantee a simple result.

### *A. Transmission Line Stubs*

Terminated transmission lines, aka 'stubs', are commonly employed in problems of impedance matching at microwave frequencies where lumped elements are not realizable. Given the operator for a lossless transmission line, the susceptance of transmission lines terminated with either a short or open circuit may be found and implemented with the susceptance rotor. The conformal vector for an open circuit in the s-domain is

$$\uparrow(e_1) = e_1 + e_4 \tag{154}$$

The susceptance of a lossless transmission line terminated in an ideal open circuit is then,

$$R_{ys}R_l\left(e_1 + e_4\right)R_l^{\sim}R_{ys}^{\sim} = \sin\left(2\theta\right)e_2 - \cos\left(2\theta\right)e_3 + e_4 \tag{155}$$

Similarly for a shorted shunt stub

$$R_{ys}R_l\left(-e_1 + e_4\right)R_l^{\sim}R_{ys}^{\sim} = -\sin\left(2\theta\right)e_2 + \cos\left(2\theta\right)e_3 + e_4 \tag{156}$$

This article has been accepted for publication in a future issue of this journal, but has not been fully edited. Content may change prior to final publication. Citation information: DOI 10.1109/ACCESS.2017.2727819, IEEE Access



Because this result occupies only three dimensions, it can be visualized. As $\theta$ varies, the susceptance of the stubs sweep out circular paths in a 3-dimensional subspace defined by the trivector $e_2 \wedge e_3 \wedge e_4$. As shown in Figure 23, the open and short stubs are vectors that rotate about the $e_4$-axis antipodally. As they cross the $E_0$-plane they pass through the $e_o$ and $e_\infty$ vectors.

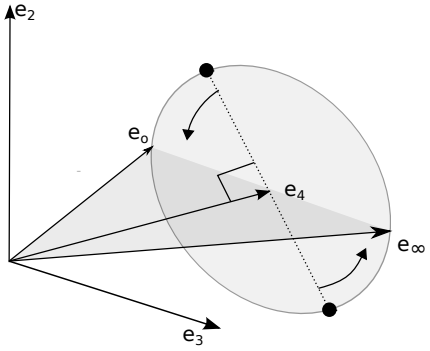


Figure 23: Subspace projection of conformal vectors representing the susceptance of shorted/opened transmission lines.

Down projecting this open stub returns the familiar formula

$$\downarrow (\sin(2\theta)\, e_2 - \cos(2\theta)\, e_3 + e_4) = \tan(\theta) e_2 \tag{157}$$

Using this result, the operator for a shunted transmission line terminated with an ideal open circuit is constructed.

$$R_{os} \equiv e^{\frac{1}{2}\tan(\theta)(e_{12}+e_{24})} \tag{158}$$

Similarly,the operator for a shunted transmission line terminated with an ideal short circuit is,

$$R_{ss} \equiv e^{-\frac{1}{2}\cot(\theta)(e_{12}+e_{24})} \tag{159}$$

Loss present within the stubs can be added by cascading the dilation rotor given in table III. For example, to add loss to the shorted shunt stub

$$e^{-\frac{1}{2}\ln\lambda e_{34}} e^{-\frac{1}{2}\cot(\theta)(e_{12}+e_{24})} \tag{160}$$

The loss factor $\lambda$ can be replaced by a function of electrical length $\theta$ if desired. More detail on lossy transmission lines is given in Section VII.

### *B. Shunt Stub Impedance Matching*

A shunt stub matching circuit provides a network topology that can match an arbitrary load impedance to some line impedance at a given frequency. The network is shown in figure 24a, where $Z_L$ is the load impedance, $Z_0$ is the line impedance, and $\theta$ and $\phi$ are the series and shunt line-lengths, respectively. The problem is to choose $\theta$ and $\phi$ so that the input reflection coefficient $\Gamma_{in}$ is zero.

The desired condition is a match at the input, i.e. a reflection coefficient of 0. Starting from this known condition, the problem may be solved in reverse by inverting the network in figure 24a to produce the network shown in figure 24b. From this orientation the matched line impedance is seen through the series transmission line, then the shunted stub. In language of operators, this *inverted* network takes $e_o$ through a $B$-rotation, then a $L$-rotation, to end up at some desired load reflection coefficient $\Gamma_L$. An illustration of the path produced by these operators, as seen projected on the Smith Chart, is shown in Figure 25. The combined operator for the network is a expressed by

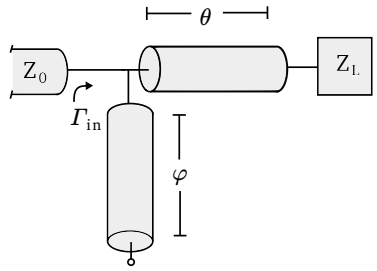


(a) Single stub matching network.

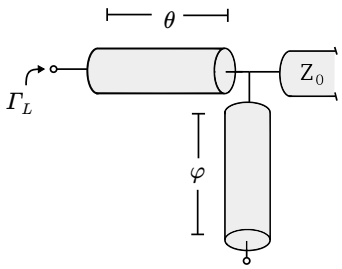


(b) Inversion of the single stub matching network.

Figure 24: Networks for single stub impedance matching

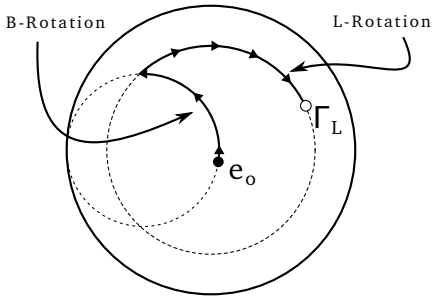


Figure 25: A possible path from $e_o$ to $\Gamma_L$ produced by the inverse shunt stub network.

$$\Gamma_L = e^{\theta e_{12}} e^{\frac{1}{2}\cot(\phi)B} e_o e^{-\frac{1}{2}\cot(\phi)B} e^{-\theta e_{12}} \tag{161}$$

Down-projecting the results gives the formula,

$$\begin{aligned}\gamma_L = \downarrow \Gamma_L \\ = -(\frac{1}{2}\cos(2\theta) + \frac{1}{2}\cos(2(\phi\text{-}\theta)))e_1 + \\ (\frac{1}{2}\sin(2\theta) - \frac{1}{2}\sin(2(\phi\text{-}\theta)))e_2\end{aligned} \tag{162}$$

Which is complicated, but by noticing that the magnitude of the reflection coefficient is only influenced by the shunt stub, taking the magnitude and angle (with respect to $e_1$) decouples the interdependence,

This article has been accepted for publication in a future issue of this journal, but has not been fully edited. Content may change prior to final publication. Citation information: DOI 10.1109/ACCESS.2017.2727819, IEEE Access



$$|\gamma_L|^2 = \frac{1}{4\tan^2(\phi)+1} \tag{163}$$

$$\tan(\angle\gamma_L) = \frac{\tan(2\theta)+2\tan(\phi)}{2\tan(2\theta)\tan(\phi)-1} \tag{164}$$

These can be inverted to give direct expressions for the stub lengths

$$\phi = \arctan\left(\frac{1}{2|\gamma_L|}\sqrt{1-|\gamma_L|^2}\right) \tag{165}$$

$$\tan(2\theta) = \frac{2\tan(\phi)+\tan(\angle\gamma_L)}{2\tan(\phi)\tan(\angle\gamma_L)-1} \tag{166}$$

### C. Impedance Transformer

A impedance transformer is a circuit topology used to match real load impedance by using $90^\circ$ section of mismatched transmission line. Given a known system and load impedance, the design goal is to determine the line impedance which creates the matched condition, $\Gamma_{\text{in}} = 0$. A circuit diagram for this topology is show in Figure 26, where $Z_0$ is the system impedance, $nZ_0$ is the transformer's line impedance, and $Z_L$ is the load.

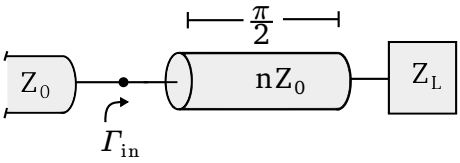


Figure 26: Network for an impedance transformer.

As described in Section VII-D, the operator for this circuit may be constructed from an impedance step, a matched line of $90^\circ$, and another impedance step of inverse magnitude.

$$\begin{aligned} R_{ml} &= \tilde{R_n} R_l R_n \\ &= e^{\frac{1}{2}\ln(n)e_{14}} e^{\frac{\pi}{2}e_{12}} e^{-\frac{1}{2}\ln(n)e_{14}} && (167) \\ &= \cosh(\ln(n))\, e_{12} + \sinh(\ln(n))\, e_{24}. && (168) \end{aligned}$$

An illustration of the path created from these operators is shown in Figure 27. By using a line of $90^\circ$, the L-rotation rotates the load by $\pi$. Proceeding in a similar way as with the single stub problem, the circuit is inverted so that the system impedance is seen through the line. This produces expressions for the normalized load impedance directly.

$$\begin{aligned} \gamma_L &= \downarrow\left(\tilde{R_{ml}} e_o R_{ml}\right) \\ &= -\tanh(\ln(n))\, e_1 \\ &= \frac{1-n^2}{1+n^2} e_1 \end{aligned} \tag{169}$$

The result is usually given in the impedance domain.

$$\begin{aligned} z_L &= \downarrow\left(R_{zs} R_{ml} e_o \tilde{R_{ml}} R_{zs}\right) \\ &= \frac{1}{n^2 e_1} \end{aligned} \tag{170}$$

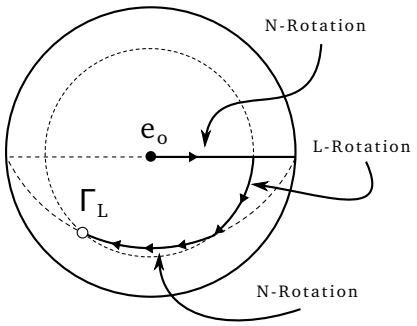


Figure 27: Path taken by a matched load as produced by a mismatched transmission line.

Which is the correct, but expressed in normalized units. To solve the more general case in which the load is not real, the same steps are applied but with the more general operator for a line of unspecified length. Down-projecting $\tilde{R_{ml}} e_o R_{ml}$ produces the equations.

$$|\gamma_L|^2 = \frac{\tan^2(\theta)\sinh^2(\ln(n))}{\tan^2(\theta)\cosh^2(\ln(n))+1} \tag{171}$$

$$\tan(\angle\gamma_L) = -\frac{1}{\tan(\theta)\cosh(\ln(n))} \tag{172}$$

These expressions are intertwined in both $\theta$ and $n$ as one would expect by looking at the Carter Chart.

## IX. Advantages of CGA

For those unfamiliar with geometric algebra, making use of our results will require a significant investment. Therefore, this section presents arguments for why the investment might be made.

*Geometric Insight :* The most important advantage of using CGA is the geometric insight it provides. The inability of complex algebra to handle more than two dimensions causes much of the structure present in transmission line theory to be hidden. For example, the normalized input impedance of a normalized load $\mathbf{z}$ as seen through a lossless transmission line is conventionally described by the following formula.

$$\frac{\mathbf{z}+j\tan(\theta)}{1+\mathbf{z}j\tan(\theta)} \tag{173}$$

This formula has no geometric interpretation. In contrast, CGA allows this relationship to represented as a rotation in the $e_{23}$ plane by an angle of $2\theta$. It has been shown how CGA naturally leads to the discrete element bivector group and non-euclidean rotations. In addition, the Smith Chart and the Riemann Sphere have been identified as part of a coherent evolution of projective geometry that eventually leads to CGA.

*Simplicity:* One criticism of the current theory is that it is more complicated than the traditional, two-dimensional theory. To reflect, the CGA framework has replaced a set of Möbius transformations in a Euclidean plane, with rotations in a 4-dimensional Minkowski space. In other words, complicated transformations in a simple space have been replaced by simple transformations in a complicated space, a

reoccurring theme in electrical engineering. The conventional two-dimensional space is simpler precisely because it fails to accurately model the sophistication of the physics. There are many cases in which usage of this simplified space is advantageous, and it is not expected that CGA will replace every instance of computation that engineers make on a daily basis. However, simplicity should not be confused with familiarity.

From a modeling perspective, the ability of the CGA operator formalism to consistently transform operators and operands is an increase in both clarity and simplicity. This property, known as *covariance*, has been demonstrated by transforming transmission line operators to different domains and in representing a mismatched transmission line as matched line that is operated on by an impedance mismatch. Additionally, this approach is more easily implemented in software.

*Scalability:* An inherent problem with the conventional theory is its lack of *scalability*. Because the individual transformations are non-linear, each additional component increases the overall complexity of a result. For example, to compute the effect of adding series resistance on the reflection coefficient using conventional theory, one does the following: take the present value of reflection coefficient $\mathbf{s}$, and transform it to the impedance domain.

$$\mathbf{z} = \frac{1+\mathbf{s}}{1-\mathbf{s}} \tag{174}$$

Next, add the resistance $r$, producing the new load impedance $\mathbf{z}'$.

$$\mathbf{z}' = \mathbf{z} + r \tag{175}$$

Then transform back into reflection coefficient, $\mathbf{s}'$.

$$\mathbf{s}' = \frac{\mathbf{z}'-1}{\mathbf{z}'+1} \tag{176}$$

Finally, compile of these operations into a single equation,

$$\mathbf{s}' = \frac{\frac{\mathbf{1}+\mathbf{s}}{\mathbf{1}-\mathbf{s}} + r - 1}{\frac{\mathbf{1}+\mathbf{s}}{\mathbf{1}-\mathbf{s}} + r + 1} \tag{177}$$

Due to this lack of scalability, the entire expression becomes uninterpretable. In response, engineers invent graphical aids such as Smith Chart. Compare eq (177) with its equivalent expression in CGA.

$$S' = e^{\frac{r}{2}(e_{34}-e_{13})} S e^{-\frac{r}{2}(e_{34}-e_{13})} \tag{178}$$

Not only does this representation separate the operand from operator, but it has a definite geometric interpretation. By supporting non-euclidean rotations, the familiar contours of the Smith Chart can be expanded to include impedance transformations, and the effects of mismatched lines. In CGA, each individual transform, as well as an arbitrary number of cascaded transforms are all represented with rotations. Therefore, once the mathematics of rotations is mastered, problems of great complexity can be tackled.

*Domain Invariance and Singularity Avoidance:* As just demonstrated, the dependence of a circuit's mathematical complexity on the choice of representation forces one to switch domains regularly. The domain invariance produced by CGA solves this problem completely. Additionally, many of the singularities caused by values of 0 and $\infty$ are removed by using CGA, regardless of the chosen domain. These singularities are removed by replacing the concept of distance with that of direction, an important feature of projective geometry.

*Universality :* It has been argued elsewhere [21] that the adoption of geometric algebra is a necessary step required to unify the splintered world of applied mathematics. We agree with this perspective and further believe that universal adoption is inevitable. At first glance, the construction presented in this paper may appear highly specialized, and applicable only to transmission line theory. However, the $G_{3,1}$ algebra is identical to the Space-Time Algebra (STA) used by physicists working with relativity. It is likely that many analogues can be made between the circuit transformations and Lorentz transformations, a topic which deserves study. In addition to the efforts of physicists, many results in CGA have been produced by engineers working in fields of computer graphics and computer vision. The universality of GA makes this type cross-disciplinary collaboration practical.

## X. Conclusion

### A. Verification and Summary of Results

The versors and their generating bivectors developed in the later sections are summarized in Table V. Many of the results presented were found using `galgebra` [22], an open-source symbolic clifford algebra module for python. `galgebra` is especially useful for many of the tedious down-projection computations. In addition, all of the results have been numerically verified to be consistent with the conventional theory, where possible. These numerical tests were done using using the open-source python module `clifford`. A git repository containing the verification suite is available online at https://github.com/arsenovic/. Questions and comments on the code are welcomed by the author.

### B. Discussion

The application of Conformal Geometric Algebra to transmission line theory has been presented. The preliminary results appear promising and justify continued development of the subject. To review, the fundamental network operations such as adding impedance or admittance elements and cascading transmission lines have been implemented with rotations in a four dimensional Minkowski space. Additionally, it has been shown that the different circuit representations: impedance, admittance, and reflection coefficient, are also related by rotations. In doing so, the majority of relationships in transmission line theory have been linearized. Common transmission line formulae have been replaced with a bivector algebra and an associated operator framework. A demonstration of the framework has been made by computing rotors for mismatched transmission lines, and solving impedance matching problems.

| Circuit | Generator | versor |
|---|---|---|
| Lossless Transmission Line | $L = e_{12}$ | $e^{\theta L}$ |
| Attenuation/Gain | $A = e_{34}$ | $e^{-\frac{1}{2}\ln \alpha A}$ |
| Resistance | $R = (e_{34} - e_{13})$ | $e^{\frac{r}{2}R}$ |
| Reactance | $X = (e_{12} - e_{24})$ | $e^{\frac{x}{2}X}$ |
| Conductance | $G = (e_{34} + e_{13})$ | $e^{\frac{g}{2}G}$ |
| Susceptance | $B = (e_{12} + e_{24})$ | $e^{\frac{b}{2}B}$ |
| Impedance Step (mag) | $N = e_{14}$ | $e^{-\frac{1}{2}\ln(n)N}$ |
| Impedance Step (phase) | $Q = -e_{23}$ | $e^{\frac{\theta}{2}Q}$ |
| Shunted Open Stub | $B$ | $e^{\frac{1}{2}\tan\theta B}$ |
| Shunted Short Stub | $B$ | $e^{-\frac{1}{2}\cot\theta B}$ |

Table V: CGA generating bivectors and versors for circuit components.

All of the results presented have been verified to be numerically consistent with the conventional theory, where possible. Finally, an argument for the adoption of the current theory has been presented, and we hope it is convincing.

### C. Future Work

We plan to follow this paper with another demonstrating continued applications of CGA transmission theory. Some areas of interest mentioned throughout this paper are transmission line classification, fixed points analysis, and active impedance matching. Other areas which we think will produce useful results are multi-section impedance transformers, periodic structures (filters), artificial transmission lines, and reflectometer calibration. Symmetric N-port structures could also be investigated, given that they are generally decomposed into a set of one-port circuits. In addition to various circuit architectures, the CGA operator framework should be useful for uncertainty propagation, given that all of the functions are reduced to rotations. A foundation for this work has already been accomplished in [23].

### D. Acknowledgements

We would like to acknowledge David Hestenes for his consistent encouragement and Allan Cortzen for his generous assistance.

## References

[1] H. Wheeler, "Reflection Charts Relating to Impedance Matching," *IEEE Transactions on Microwave Theory and Techniques*, vol. 32, pp. 1008–1021, Sept. 1984.

[2] A. Muller, P. Soto, D. Dascalu, D. Neculoiu, and V. Boria, "A 3-D Smith Chart Based on the Riemann Sphere for Active and Passive Microwave Circuits," *IEEE Microwave and Wireless Components Letters*, vol. 21, pp. 286–288, June 2011.

[3] M. Gupta, "Escher's art, Smith chart, and hyperbolic geometry," *IEEE Microwave Magazine*, vol. 7, pp. 66–76, Oct. 2006.

[4] E. F. Bolinder and A. F. C. R. C. U. S. . E. R. Directorate, *Impedance, Power, and Noise Transformations by Means of the Minkowski Model of Lorentz Space*. Electromagnetic Radiation Laboratory, Electronics Research Directorate, Air Force Cambridge Research Center, Air Research and Development Command, United States Air Force, 1959.

[5] E. Bolinder, "Unified Microwave Network Theory Based on Clifford Algebra in Lorentz Space," in *Microwave Conference, 1982. 12th European*, pp. 25–35, Sept. 1982.

[6] E. Bolinder, "Clifford algebra: What is it?," *IEEE Antennas and Propagation Society Newsletter*, vol. 29, pp. 18–23, Aug. 1987.

[7] J. Chappell, S. Drake, C. Seidel, L. Gunn, A. Iqbal, A. Allison, and D. Abbott, "Geometric Algebra for Electrical and Electronic Engineers," *Proceedings of the IEEE*, vol. 102, pp. 1340–1363, Sept. 2014.

[8] C. Doran, *Geometric Algebra for Physicists*. Cambridge; New York: Cambridge University Press, 1st pbk. ed. with corr edition ed., Nov. 2007.

[9] L. Dorst, *Geometric Algebra for Computer Science*. Amsterdam; San Francisco: Morgan Kaufmann, 1 edition ed., Apr. 2007.

[10] L. Dorst, "The Construction of 3d Conformal Motions," *Mathematics in Computer Science*, Mar. 2016.

[11] S. Mann and L. Dorst, "Geometric algebra: a computational framework for geometrical applications. 2," *IEEE Computer Graphics and Applications*, vol. 22, pp. 58–67, July 2002.

[12] L. Dorst and S. Mann, "Geometric Algebra: A computational framework for geometrical applications Part 1," *IEEE Computer Graphics and Applications*, vol. 22, pp. 24–31, May 2002.

[13] J. Zamora and E. Bayro-Corrochano, "Inverse kinematics, fixation and grasping using conformal geometric algebra," in *Intelligent Robots and Systems, 2004. (IROS 2004). Proceedings. 2004 IEEE/RSJ International Conference on*, vol. 4, pp. 3841–3846 vol.4, Sept. 2004.

[14] D. Hestenes, *New Foundations for Classical Mechanics*. Dordrecht; Boston: Springer, 2nd edition ed., Sept. 1999.

[15] D. Hestenes, "The design of linear algebra and geometry," *Acta Applicandae Mathematica*, vol. 23, pp. 65–93, Apr. 1991.

[16] K. J. Sangston, "Geometry of complex data," *IEEE Aerospace and Electronic Systems Magazine*, vol. 31, pp. 32–69, Mar. 2016.

[17] T. Needham, *Visual Complex Analysis*. Oxford; New York: Oxford University Press, USA, new ed edition ed., Feb. 1999.

[18] J. Vince, *Geometric Algebra for Computer Graphics*. London: Springer, 2008 edition ed., Apr. 2008.

[19] D. H. C. Doran, "Lie groups as spin groups," *Journal of Mathematical Physics*, vol. 34, no. 8, 1993.

[20] D. Hestenes, *Space-Time Algebra*. Cham: Springer International Publishing, 2015.

[21] D. Hestenes, "A Unified Language for Mathematics and Physics," in *Clifford Algebras and Their Applications in Mathematical Physics* (J. S. R. Chisholm and A. K. Common, eds.), no. 183 in NATO ASI Series, pp. 1–23, Springer Netherlands, Jan. 1986.

[22] A. Bromborsky *et al.*, "galgebra," 2009.

[23] C. Perwass, *Geometric Algebra with Applications in Engineering*. Springer, softcover reprint of hardcover 1st ed. 2009 ed., Nov. 2010.

**Alex Arsenovic** received a B.S and Ph.D in Electrical Engineering from the University of Virginia in 2007 and 2012, respectively. While completing his Ph.D. thesis on microwave metrology, he created the open-source package `scikit-rf` and has been actively developing it since 2009. Alex has worked as an independent consultant in Central Virginia for the past 4 years, with clients such as Virginia Diodes Inc, Nuvotronics, and Plotly. He continues to work closely with the University of Virginia, and has authored and co-authored over 15 technical papers in the field of microwave metrology and calibration. In 2016, he created Eight Ten Labs LLC (www.810lab.com) to continue providing the services for microwave metrology, software development, and applied mathematics. Currently, he is working on reformulating microwave network theory in the language of geometric algebra. This is part of a larger project to modernize the theoretical and computation tools used by microwave and electrical engineers.